Exploiting Collective Effects in a System of Interacting Quantum Emitters

Masterarbeit

zur Erlangung des akademischen Grades
Master of Science
(MSc)

eingereicht an der
Fakultät für Mathematik, Informatik und Physik
der Universität Innsbruck

von
David Plankensteiner, BSc

Betreuer:
Univ. Prof. Dr. Helmut Ritsch

Mitwirkender Betreuer:
Dr. Claudiu Genes

Institut für Theoretische Physik

Innsbruck, am 24 November 2014

Abstract

We study a chain of closely spaced two-level atoms subject to dipole-dipole interactions and collective decay. Phenomena like super-radiance can occur, which is physically very interesting but detrimental in many applications, including Ramsey or Rabi spectroscopy. Advanced control and manipulation of the collective effects is therefore of interest.
We first advance a proposal that allows for the exploitation of the mutual interactions in order to reduce the collective decay. This is done by modifying the symmetry of the states of the system via manipulation of the individual phases of each atom in the chain. This reduces the collective decay rate exponentially with the atom number N, i.e. the system becomes more sub-radiant by adding more atoms to the chain.
In a first step, we distribute the individual phases equally among the atoms in the chain in order to achieve maximal asymmetry. The resulting states are then used in the well-known Ramsey spectroscopy. We show that, using these asymmetric states, the resulting signal sensitivity exhibits a scaling with N that shows an improvement over the case of independently decaying atoms ($1/\sqrt{N}$).
The same method of phase-spreading is used to protect a multipartite entangled state (spin-squeezed state) against decay. Analytical results for two interacting atoms are explicitly calculated and yield favourable results. Dynamics of larger systems are computed numerically.
Up to this point, the coherent part of the dipole-dipole interaction in the atom chain does not play a major role. In the last part of the thesis, however, we suggest a technique that involves making use of the energy shifts that are introduced by the mutual dipole-dipole interaction. Specifically, the most robust multipartite state is identified and energetically separated from shorter-lived states. This separation gets larger by a reduction of the interatomic distance, i.e. by increasing the dipole-induced energy shifts. Phases similar to the ones used in the previous applications are directly imprinted on the system by a proper design of the driving laser's configuration. This method essentially allows for the application of a π-pulse on the system (initially in the ground state) in order to coherently transfer the population into the most robust state. Finally, an experimental realization employing a magnetic field gradient yielding time-dependent phases is discussed. Numerical simulations of the dynamics of the system validate the efficiency of the suggested procedure.

Zusammenfassung

Wir untersuchen eine Kette dicht gedrängter Zwei-Niveau Atome, in der Dipol-Dipol Wechselwirkung und kollektiver Zerfall von Relevanz sind. Zweiteres führt zu Phänomenen wie etwa Super-Radianz, die in vielen Anwendungen, darunter Ramsey und Rabi Spektroskopie, einen unvorteilhaften Einfluss haben. Daher ist ein besseres Verständnis und die Kontrolle über diese kollektiven Effekte von größtem Interesse. Zu diesem Zweck wird eine Kette von äquidistanten Zwei-Niveau Atomen untersucht.
Eine Methode, die es erlaubt die gegenseitige Wechselwirkung der Atome auszunutzen, um den kollektiven Zerfall zu reduzieren, wird gezeigt. Dies kann durch einen Bruch der Symmetrien der Zustände des Systems erreicht werden, welcher wiederum durch Manipulation der individuellen Phase eines jeden Atoms in der Kette herbeigeführt wird. Im Anschluss wird gezeigt, dass dieser reduzierte kollektive Zerfall des Ensembles mit steigender Anzahl von Atomen N exponentiell abnimmt, was effektiv bedeutet, dass die Sub-Radianz des Systems durch hinzufügen neuer Atome zu der Kette weiter gefördert wird.
Als ein erstes Beispiel für die Vorteile, die eine solche Zerfallsreduktion bietet, werden die Einzelphasen von Zuständen, die in der gemeinhin bekannten Methode der Ramsey Spektroskopie verwendet werden, gleichverteilt, um maximale Asymmetrie zu erzeugen. Mit Hilfe dieser neuen, asymmetrischen Zustände, wird dann gezeigt, dass man eine Skalierung der resultierenden Signalgenauigkeit mit der Atomzahl erreichen kann, die über den Fall unabhängig zerfallender Atome ($1/\sqrt{N}$) hinausgeht.
Für die selbe Art der Phasenverteilung wird eine weitere Anwendung präsentiert, nämlich der Schutz eines verschränkten Vielteilchen-Zustandes (Spin-Squeezed Zustand) vor Zerfall. Im Zuge dessen werden analytische Ergebnisse für zwei wechselwirkende Atome hergeleitet, welche die Vorteile von phasenverteilten Zuständen verdeutlichen. Diese Ergebnisse werden dann durch numerische Simulationen auf Ketten mehrerer Atome ausgeweitet.
In den bis zu diesem Punkt diskutierten Anwendungen war die Dipol-Dipol Wechselwirkung der Atome in der Kette nur ein störender Faktor von geringer Relevanz. Im letzten Teil dieser Arbeit wird jedoch ein Vorschlag unterbreitet, wie man die Energieverschiebungen, die in den Energieniveaus durch die Wechselwirkung der Dipole induziert werden, ausnutzen kann, um einen äußerst robusten Vielteilchen-Zustand zu präparieren. Hierbei wird zuerst der Zustand mit der längsten Lebensdauer identifiziert und es wird gezeigt, dass man ihn durch eine Reduktion der Distanz zwischen den Atomen in der Kette, was effektiv einer drastischen Zunahme der Wechselwirkung der atomaren Dipole entspricht, energetisch von den restlichen Zuständen separieren kann. Nachdem diese Separation geschehen ist, kann man den Zustand energetisch ansprechen, jedoch müssen weiters noch Phasen, ähnlich denen, die in den vorigen Anwendungen verwendet wurden, direkt über den treibenden Laser auf das System übertragen werden, um die Symmetrie der Anregung an die Asymmetrie dieses langlebigen Zustandes anzupassen. Diese Methode macht es möglich, einen π-Puls auf das System (welches anfänglich im Grundzustand

ist) anzuwenden, sodass sich dieses dann in dem Zustand mit der geringsten Zerfallsrate befindet. Zuletzt wird diskutiert, wie man solche Phasen in einem treibenden Laser experimentell realisieren könnte. Dies kann mit Hilfe eines Magnetfeldgradienten erreicht werden, dessen induzierte Energieverschiebungen äquivalent zu zeitabhängigen Phasen sind. Numerische Simulationen der Dynamik des Systems bestätigen die Effizienz der vorgeschlagenen Prozedur.

Danksagungen

Als erstes möchte ich meinen Eltern danken. Spezieller Dank gilt meiner Mutter, auf deren Unterstützung ich sowohl in der Schul- als auch Studienzeit zählen konnte. Weiters konnte ich mich auf meine beiden Schwestern und meine gesamte Verwandtschaft in der Ackergasse voll und ganz verlassen.
Außerdem gebührt natürlich sämtlichen Mitgliedern der Arbeitsgruppe Dank für die freundliche Aufnahme und das gute Arbeitsklima. Ganz besonders möchte ich mich bei Claudiu Genes bedanken, der immer für Fragen offen war und es immer geschafft hat mich für die Arbeit zu begeistern. Gleiches gilt für Laurin Ostermann, ohne dessen Hilfe ich wahrscheinlich immer noch versuchen würde, einen Programmierfehler zu finden. Selbstverständlich wäre all dies nicht ohne meinen Betreuer, Prof. Helmut Ritsch, möglich gewesen, dem es überhaupt erst zu verdanken ist, dass ich an einem so interessanten Thema arbeiten durfte.
Zu guter Letzt möchte ich mich auch ganz herzlich bei meinen guten Freunden bedanken, die mich in jeder Lebenslage begleitet haben.
Abschließend sei noch einmal allen Genannten und nicht Genannten gedankt, wobei letztere hoffentlich nicht zu viele sind.

We acknowledge the use of the open source software QuTiP 2.2. [1] for the numerical investigations of the system dynamics in the various applications throughout this thesis.

Contents

Chapter 1

Introduction

There are many modern research fields such as quantum metrology [2] and quantum information processing [3] where technology has reached the level at which the most fundamental effects of interaction between atoms in an ensemble is of significant relevance. It has hence recently been of growing interest to further the understanding of those fundamental effects and learn how to control, manipulate and even use them to our advantage. There have been recent proposals [4, 5] as how to reduce the collective emission, which often is a limiting factor, by manipulating the phases of each emitter in an ensemble individually.
The purpose of this thesis is to analyze and exploit collective effects of quantum emitters in possible applications. While mutual decay and dipole-dipole interactions are described for more general systems, the discussion is soon restricted to a chain of two-level atoms with a small interatomic distance (lattice constant). Still, such a chain configuration already has a vast amount of applications, some of which that are also discussed in this thesis, such as Ramsey spectroscopy, state protection and preparation.
First, the theoretical premise for the treatment of the system is set in Chapter 2. After a brief discussion of the quantum mechanical model of an ensemble of two-level atoms, the time dependent dynamics are presented. The time evolution is computed via the well-known master equation, which is characterized by a Hamiltonian operator that is defined beforehand and a Liouvillian superoperator in standard Lindblad form. The interatomic interaction in the chain consists of dipole-dipole interaction as well as mutual decay. While the dipole shifts are included in the dynamics by a respective term in the Hamiltonian, the mutual decay rates are the dissipative rates in the Liouvillian. These collective effects are discussed for two-level atoms in an arbitrary geometry, just before the restriction to a chain configuration is made.
Afterwards, the mutual decay rates are used as elements of a matrix and it is established that the states of the system under consideration can only decay through certain channels (decay channels) with rates that are the eigenvalues of this matrix. The scaling of these rates, specifically the minimal and maximal one, with an increasing number of atoms is investigated. The results gained for various applications throughout the thesis

are compared to this scaling.
Once the framework of decay has been presented, an idea as how to reduce the collective decay by breaking the symmetry of the states under consideration is provided. This is done by individual manipulation of the phase of each atom in the chain. A corresponding proposal will be the main concern of the thesis. To further motivate the effectiveness of reducing the symmetry, states with equally distributed phases containing only one excitation are considered. Even though those states are not, in general, eigenstates of the system Hamiltonian, they form a basis in the subspace of single excitation states. Furthermore, it is shown that the phase-spread states become eigenstates of the system in the limit of extremely small lattice constants in the chain [6]. The derivation of an analytical expression for the decay rates of these states is presented and the minimal and maximal decay rates are compared to the eigenvalues of the decay rate matrix. To conclude this chapter, the previously discussed proposal of phase distribution is formulated once again in terms of rotations on the Bloch sphere that can be applied to an arbitrary state of the atomic chain in order to reduce its symmetry.
The following chapters each present one specific application where favourable results due to the proposed reduction of symmetry and decay are gained. Chapter 3 and 4 discuss applications in which the phase-spread rotations that have been previously defined are proven to be of great use. Namely, chapter 3 contains a brief discussion of Ramsey spectroscopy, which is a well established method in quantum metrology. The fact that the emission rate is a limiting factor in the signal sensitivity of this spectroscopic method makes the proposed reduction of decay highly desirable. Numerical methods are applied in order to show that application of the phase-spread rotations does indeed yield better results than when following the common method of Ramsey spectroscopy.
In chapter 4, on the other hand, preparation of an entangled state in form of a spin squeezed state is discussed. It is then shown that by applying the same phase-spread rotations once again, one can even protect the entanglement in such a state against decay. This, of course, is also highly desirable since entanglement is an expensive resource in quantum processing.
Chapter 5 contains a new proposal. Instead of preparing a state and then applying an operation of phase-distribution in order to reduce its decay rate, the aim in this chapter is the direct preparation of a robust state [7]. This is done by first numerically identifying the state with the lowest decay rate. The dipole-dipole interactions can then be used in order to produce energetic shifts lifting the degeneracy in the single-excitation subspace and are eventually large enough to energetically separate the states from one another far enough to be able to specifically address this state. Since the state under consideration is asymmetric, the laser used to drive the system has to imprint this asymmetry in the form of phases similar to the ones previously defined in the context of the phase-spread rotations. In order to demonstrate the working principle of such an asymmetric driving, the phases that need to be imprinted are artificially included in the Hamiltonian that describe the exciting laser. The optimal phases turn out to be the same ones used in the phase-spread rotations and the efficiency of the procedure

is confirmed by numerical results. Once the general motivation has been given and sufficiently justified, a proposal as how to experimentally realize such a phase imprinting driving is discussed. Specifically, this can be achieved by utilizing a magnetic field gradient, which shifts the single atom excited states progressively. This is motivated by a brief analytical discussion, followed by application of numerical methods, again showing great efficiency of the procedure.
Chapter 6 offers general conclusions and an outlook on future matters of research.

Chapter 2

Theoretical Concepts

In this chapter a detailed description of an ensemble of quantum emitters and the collective decay of such a system is provided. For the mathematical description it is irrelevant if said ensemble consists of two-level atoms or spin-1/2 particles or any other sort of emitter, since the dynamics are equivalent from a mathematical point of view. For example, choosing these emitters to be two-level atoms simply manifests itself on the labelling of the levels of these emitters. Namely, from here on out the levels of a single emitter shall be called $|g\rangle$ for the ground state and $|e\rangle$ for the excited state.
The collective effects of such an ensemble of atoms consist of the mutual decay but also the dipole-dipole interaction. The strength of both of these depends on the geometry of the arrangement of the atoms. The simplest, yet unrealistic case would be to assume equal coupling between all atoms. This, however, makes little sense for a detailed discussion. The focus will therefore be on a little more involved case, namely a chain configuration with equal distance between all atoms.

2.1 System Hamiltonian and Eigenstates

Describing an ensemble of two-level atoms is mathematically equivalent to describing an ensemble of spin-1/2 particles. Therefore, the states and energies of a single atom are eigenstates and eigenvalues of the σ_z Pauli-Matrix,

$$\begin{aligned} \sigma_z |e\rangle &= |e\rangle \,, \\ \sigma_z |g\rangle &= -|g\rangle \,. \end{aligned} \tag{2.1}$$

Note, that the eigenvalues here are to be taken in units of the quantized spin $\frac{\hbar}{2}$, i.e. an atom in the excited state corresponds to a spin-1/2 particle with a spin of $\frac{\hbar}{2}$ aligned in the z-direction.
Further dynamics of a single atom can be described by the remaining Pauli-Matrices,

namely

$$\sigma^{\pm} = \frac{1}{2}(\sigma_x \pm i\sigma_y), \tag{2.2}$$
$$\sigma^{+}\left|g\right\rangle = \left|e\right\rangle, \quad \sigma^{-}\left|e\right\rangle = \left|g\right\rangle.$$

The operators σ^+ and σ^- are called *raising* and *lowering* operator, respectively.
An ensemble of N such atoms span a Hilbert space of dimension 2^N, i.e. operators in that space are $2^N \times 2^N$ matrices, including the system Hamiltonian. Neglecting the dipole-dipole interaction, this Hamiltonian has the simple form

$$H_0 = \frac{\omega_0}{2}\sum_{i=1}^{N}\sigma_z^{(i)}, \tag{2.3}$$

where ω_0 is the transition frequency of one atom. The additional index i of the operator $\sigma_z^{(i)}$ denotes that the operator σ_z is applied to the $i-th$ particle only, namely

$$\sigma_z^{(i)} = \mathbb{1}_{2^{(i-1)}} \otimes \sigma_z \mathbb{1}_{2^{(N-i)}}. \tag{2.4}$$

Here, $\mathbb{1}_n$ is simply the identity matrix of dimension $n \times n$. It is obvious that the eigenstates of the Hamiltonian in (2.3) are simply tensor products of the single atom states. The corresponding eigenvalues are also just a sum over the eigenvalues of σ_z of the state of each atom,

$$H_0\left|ege...g\right\rangle = \omega_0(\frac{1}{2} - \frac{1}{2} + \frac{1}{2} + ... - \frac{1}{2})\left|ege...g\right\rangle. \tag{2.5}$$

Here, the short form of the tensor product was used, i.e. $|ege...g\rangle = |e\rangle\otimes|g\rangle\otimes|e\rangle\otimes...\otimes|g\rangle$. It is also obvious that there are 2^N such states, spanning the entire Hilbert space as it must be the case for an eigenbasis of a hermitian operator.
However, things are not quite as simple. To fully describe the coherent dynamics of the system one needs to account for dipole-dipole interaction between the atoms. This is described by the dipole Hamiltonian

$$H_{dip} = \sum_{j\neq k}\Omega_{jk}\sigma_j^{+}\sigma_k^{-}, \tag{2.6}$$

yielding a complete system Hamiltonian of

$$H = H_0 + H_{dip} = \frac{\omega_0}{2}\sum_{j=1}^{N}\sigma_z^{(j)} + \sum_{j\neq k}\Omega_{jk}\sigma_j^{+}\sigma_k^{-}. \tag{2.7}$$

This newly introduced dipole Hamiltonian is responsible for coherent energy transfer between the atoms. The discussion of the strength of the dipole-dipole interaction, namely the Ω_{jk} in (2.6), will be given in the following section. For now, the predominant

problem shall be the fact that this Hamiltonian does not share the simple eigenstates of H_0, i.e. $[H_0, H_{dip}] \neq 0$. As it will be shown later, an analytical computation is not possible except for some special cases. This is due to the form of the Ω_{jk}.
Assuming an equal strength of dipole-dipole interaction between all atoms of the ensemble, i.e. $\Omega_{jk} = \Omega \; \forall \; j \neq k$, as is the case for two atoms, it is possible to rewrite the Hamiltonian in terms of the collective operators S_z and S^2. These are defined as

$$\begin{aligned} S_\nu &= \frac{1}{2}\sum_{i=1}^{N} \sigma_\nu^{(i)}, \quad \text{where } \nu \; \in \; \{x, y, z\}, \\ S^2 &= S_x^2 + S_y^2 + S_z^2. \end{aligned} \tag{2.8}$$

Therefore, eigenstates of the system are common eigenstates of two collective operators. Such states are more commonly known as *Dicke states* [8]. They are denoted by $|S, M\rangle$, where $S = \frac{N}{2}$ and $|M| \leq S$, such that

$$\begin{aligned} S^2 \, |S, M\rangle &= S(S+1) \, |S, M\rangle \, , \\ S_z \, |S, M\rangle &= M \, |S, M\rangle \, . \end{aligned} \tag{2.9}$$

The eigenvalue S is more commonly thought of as the size of the collective spin of a state, while M is just the total of spin-1/2 particles aligned in the z-direction. The ground state is the one where all spins point downwards in the z-direction, i.e. $|S = \frac{N}{2}, M = -\frac{N}{2}\rangle$, since this state corresponds to the minimal eigenvalue of H_0 (lowest energy). In the picture of two-level atoms, the ground state, of course, contains zero excitations.
Note, that for simplicity the Hilbert space is usually restricted to the symmetric states where $S = \frac{N}{2}$, reducing the dimension from 2^N to just $N + 1$. In this context *symmetric* is synonymous for invariant under swapping of particles. For example, the symmetric state containing a single excitation is

$$|\frac{N}{2}, -\frac{N}{2} + 1\rangle = \frac{1}{\sqrt{N}} \sum_{j=1}^{N} \sigma_j^+ \, |G\rangle \, , \tag{2.10}$$

where $|G\rangle = |g\rangle^{\otimes N}$ is the collective ground state. Unfortunately, this symmetric description is not sufficient for any further treatment of the underlying Hamiltonian from (2.7). Hence, one needs to include the asymmetric states in the description, which are highly degenerate, in order to describe the entire Hilbert space of dimension 2^N. Even though the DIcke states are not eigenstates of the general system Hamiltonian, their similarity and symmetry properties can be helpful in further discussions. Specifically, it will be shown that states of lower symmetry decay much slower than those of high symmetry. This will later coin the terms *sub-radiance* and *super-radiance*, respectively.
In conclusion of this brief introductory discussion, it is important to again state that the eigenstates of our system cannot be expressed analytically due to reasons that will become clear in the following.

2.2 Collective Dynamics

It is clear that atoms in an ensemble with dipole-dipole interaction cannot be treated independently. The strength of the interaction of the atoms depends on the type of atoms as well as their geometry. As before, our treatment will be restricted to identical two-level atoms. First, a description of collective effects will be given for arbitrary geometries, though later on the main focus will lie in the investigation of an atomic chain.
As will be seen in the following, both the collective dipole-dipole coupling and the mutual decay of the atoms can be included by describing the dynamics of our system via a Master Equation.

2.2.1 Description of Dissipation - Master Equation

The time evolution of a state with density matrix ρ of a lossless system with Hamiltonian H can be computed via a unitary time evolution operator, i.e. the time-dependent Schrödinger equation. This way of computing the time evolution is equivalent to

$$\frac{\partial \rho}{\partial t} = i[\rho, H]. \tag{2.11}$$

Note, that for our specific system the dipole-dipole interaction that is included in H, couples the 4^N differential equation gained for the densitiy matrix elements.
Losses of the system can be regarded by introducing dissipative terms in the above equation [9],

$$\frac{\partial \rho}{\partial t} = i[\rho, H] + \sum_{j,k} \left(C_j \rho C_k^\dagger - \frac{1}{2}(C_j^\dagger C_k \rho + \rho C_j^\dagger C_k) \right), \tag{2.12}$$

where the operators C_j are collapse operators that describe the dissipation of the system. The additional term introduced in (2.12) can be written as superoperator $\mathcal{L}[\rho]$ and is called *Liouville* operator. Equation (2.12) then reads

$$\frac{\partial \rho}{\partial t} = i[\rho, H] + \mathcal{L}[\rho] \tag{2.13}$$

and is called *Master* equation[1].
For our setup, i.e. damping rates $[\Gamma_{ij}]_{i,j=1}^N$, we can define a Liouvillian in standard Linblad form in order to describe the losses in the system dynamics [3],

$$\mathcal{L}[\rho] = \sum_{i,j=1}^{N} \frac{\Gamma_{ij}}{2}(2\sigma_i^- \rho \sigma_j^+ - \sigma_i^+ \sigma_j^- \rho - \rho \sigma_i^+ \sigma_j^-). \tag{2.14}$$

[1] For a thorough derivation of the Master equation, please refer to [9][10]

The rates Γ_{ij} are generalized spontaneous emission rates including the mutual coupling of the i-th and j-th atom. Obviously, $\Gamma_{ij} = \Gamma_{ji}\ \forall\ i, j$ and $\Gamma_{ii} = \Gamma$ is the single atom decay rate.
Just as it was the case for the dipole-dipole interaction (Ω_{ij}), the decay rates Γ_{ij} are of no simple form. The respective functions to compute both the dipole-dipole shifts and mutual decay rates will be briefly presented and discussed in the following.

2.2.2 Dipole-Dipole Interaction and Decay

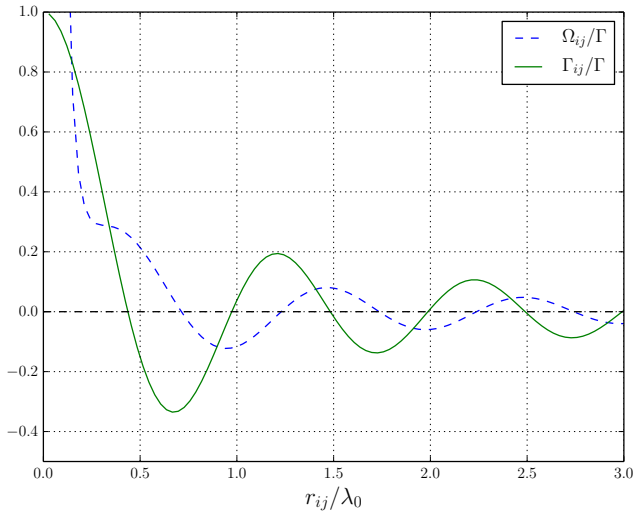

Figure 2.1: *Dipole-dipole coupling and collective emission rates.* Both Ω_{ij} and Γ_{ij} have been plotted in units of the single atom decay rate Γ as functions of the interatomic distance r_{ij} in units of the transition wavelength λ_0 at $\theta = \frac{\pi}{2}$, i.e. $\alpha = 0$.

The strength of the interaction among atoms is subject to multiple parameters. Given that all atoms have the same dipole moment $\boldsymbol{\mu}$, both the dipole-dipole interaction Ω_{ij} and the mutual decay rates Γ_{ij} depend on the system's geometry and the relative angle of this dipole moment θ to said geometry. When Γ is the single atom decay rate and $r_{ij} = |\boldsymbol{r}_i - \boldsymbol{r}_j|$ denotes the norm of the relative position vector of atom i and j, the dipole-dipole shifts and decay rates can be computed as [3]

$$\Omega_{ij} = -\frac{3\Gamma}{4}\left(\left(1-\alpha^2\right)\frac{\cos k_0 r_{ij}}{k_0 r_{ij}} - \left(1-3\alpha^2\right)\left(\frac{\sin k_0 r_{ij}}{(k_0 r_{ij})^2} + \frac{\cos k_0 r_{ij}}{(k_0 r_{ij})^3}\right)\right), \tag{2.15}$$

$$\Gamma_{ij} = \frac{3\Gamma}{2}\left(\left(1-\alpha^2\right)\frac{\sin k_0 r_{ij}}{k_0 r_{ij}} + \left(1-3\alpha^2\right)\left(\frac{\cos k_0 r_{ij}}{(k_0 r_{ij})^2} - \frac{\sin k_0 r_{ij}}{(k_0 r_{ij})^3}\right)\right). \tag{2.16}$$

The parameter $k_0 = \frac{\omega_0}{c}$ is just the transition wave number and $\alpha = \cos\theta$. Note, that both these functions go to zero for $k_0 r_{ij} \to \infty$, yet Ω_{ij} diverges, while $\Gamma_{ij} \to \Gamma$ for

$k_0 r_{ij} \to 0$ (See also [11]).
Let us mention, that from this point on a chain configuration of these atoms will be considered, with all dipole moments orthogonal to the direction of the chain, i.e. $r_{ij} = a|i-j|$, where a is the distance between nearest neighbour atoms (lattice constant), and $\alpha = 0$ (See Fig. 2.1). Note also that the main concern lies with systems of positive coupling, i.e. chain configurations where $a < 0.5\lambda_0$.

2.2.3 Decay Channels

In a physical picture the mutual decay rates Γ_{ij} are difficult to grasp. A more simplistic view will therefore be presented. The system can only collectively decay through certain channels with their respective decay rates (See Fig. 2.2). Mathematically these rates are simply the eigenvalues of the matrix with elements $[\Gamma_{ij}]_{i,j=1}^{N}$.

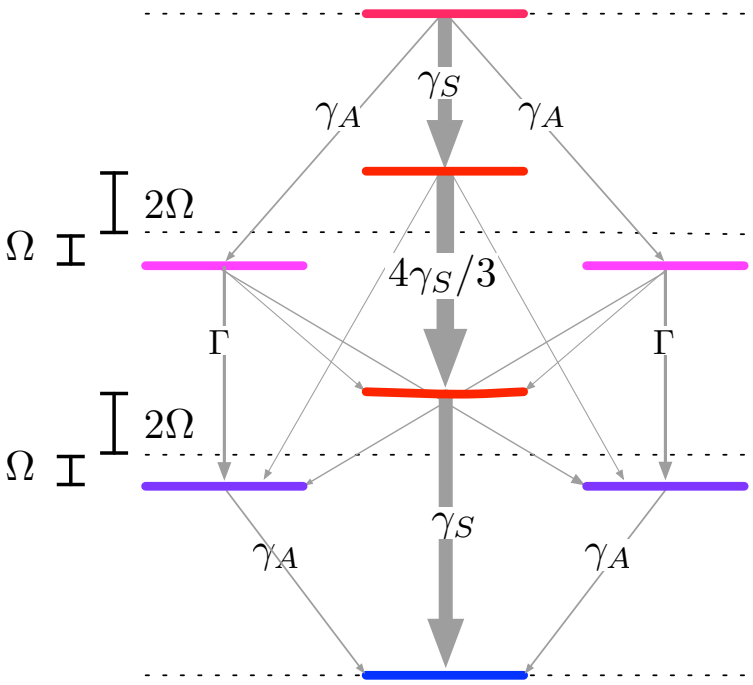

Figure 2.2: *Schematics of the decay channels for three atoms.*[2]The schematic shows the decay channels for 3 atoms in a configuration of mutual coupling, namely a triangle, such that $\Gamma_{ii} = \Gamma$, $\Gamma_{12} = \Gamma_{13} = \gamma$, $\gamma_S = \Gamma + 2\gamma$ and $\gamma_A = \Gamma - \gamma$.

[2]Schematics by Laurin Ostermann, Institut für Theoretische Physik, Universität Innbsruck, Technikerstrasse 25, A-6020 Innsbruck, Austria

In order to show that a system in a state described by a density matrix ρ actually does decay only through such channels, one has to investigate the Liouvillian from (2.14).
Since all elements in the previously mentioned decay rate matrix are real and non-zero, it is possible to find a real and orthogonal matrix, that shall be called T, which diagonalizes said matrix,

$$\sum_{i,j=1}^{N} (T^{-1})_{ki}\Gamma_{ij}T_{jl} = \sum_{i,j=1}^{N} T_{ik}\Gamma_{ij}T_{jl} = \gamma_k\delta_{kl}. \tag{2.17}$$

Here, γ_k is the k-th eigenvalue of the decay matrix. Transforming the raising and lowering operators $\sigma^{\pm}$ in the same way leads to another set of such operators working in the basis where the decay matrix is diagonal. These operators can be defined as

$$\Pi_k^{\pm} := \sum_i (T^{-1})_{ki}\sigma_i^{\pm}. \tag{2.18}$$

Inverting this definition

$$\sigma_i^{\pm} = \sum_k T_{ik}\Pi_k^{\pm}, \tag{2.19}$$

one can express the raising and lowering operators in terms of these new operators and replace them in (2.14), yielding

$$\begin{aligned}\mathcal{L}[\rho] &= \sum_{\substack{i,j=1\\k,l=1}}^{N} \frac{\Gamma_{ij}}{2}(2T_{ik}\Pi_k^-\rho T_{jl}\Pi_l^+ - T_{ik}\Pi_k^+T_{jl}\Pi_l^-\rho - \rho T_{ik}\Pi_k^+T_{jl}\Pi_l^-)\\ &= \sum_{\substack{i,j=1\\k,l=1}}^{N} \frac{T_{ik}\Gamma_{ij}T_{jl}}{2}(2\Pi_k^-\rho\Pi_l^+ - \Pi_k^+\Pi_l^-\rho - \rho\Pi_k^+\Pi_l^-).\end{aligned} \tag{2.20}$$

Making use of (2.17), this becomes

$$\mathcal{L}[\rho] = \sum_{k=1}^{N} \frac{\gamma_k}{2}(2\Pi_k^-\rho\Pi_k^+ - \Pi_k^+\Pi_k^-\rho - \rho\Pi_k^+\Pi_k^-), \tag{2.21}$$

which can be called a standard Linblad Liouvillian in decay channel form. This also clearly shows that the dissipation of a state can be written in terms of such channels that decay with a rate that is an eigenvalue of the decay matrix.

2.2.4 Scaling Laws of Decay Rates

Now that we have established that the system decays with rates that are the eigenvalues (or a superposition of them) of the decay matrix, the investigation can be extended to

questions of scaling. Once again due to the non-periodic functions that are needed to compute the elements of the decay matrix, analytical treatment is limited. However, it is quite a simple numerical task to discuss the scaling of the minimal and maximal decay rate with the atom number N, since it only requires the diagonalization of a matrix with dimensions $N \times N$. These values will represent a theoretical limit to the minimization (sub-radiance) and maximization (super-radiance) of the decay rates of the treated system. They are only a theoretical limit due to the fact that they represent the decay rates of the respective channel, but do not account for excitations due to interaction and coherent population redistribution due to dipole-dipole interaction. Still the limits can be presented, and in later sections it will be investigated how close one can get when running numerical simulations for a realistic system setup (See Fig. 2.3).

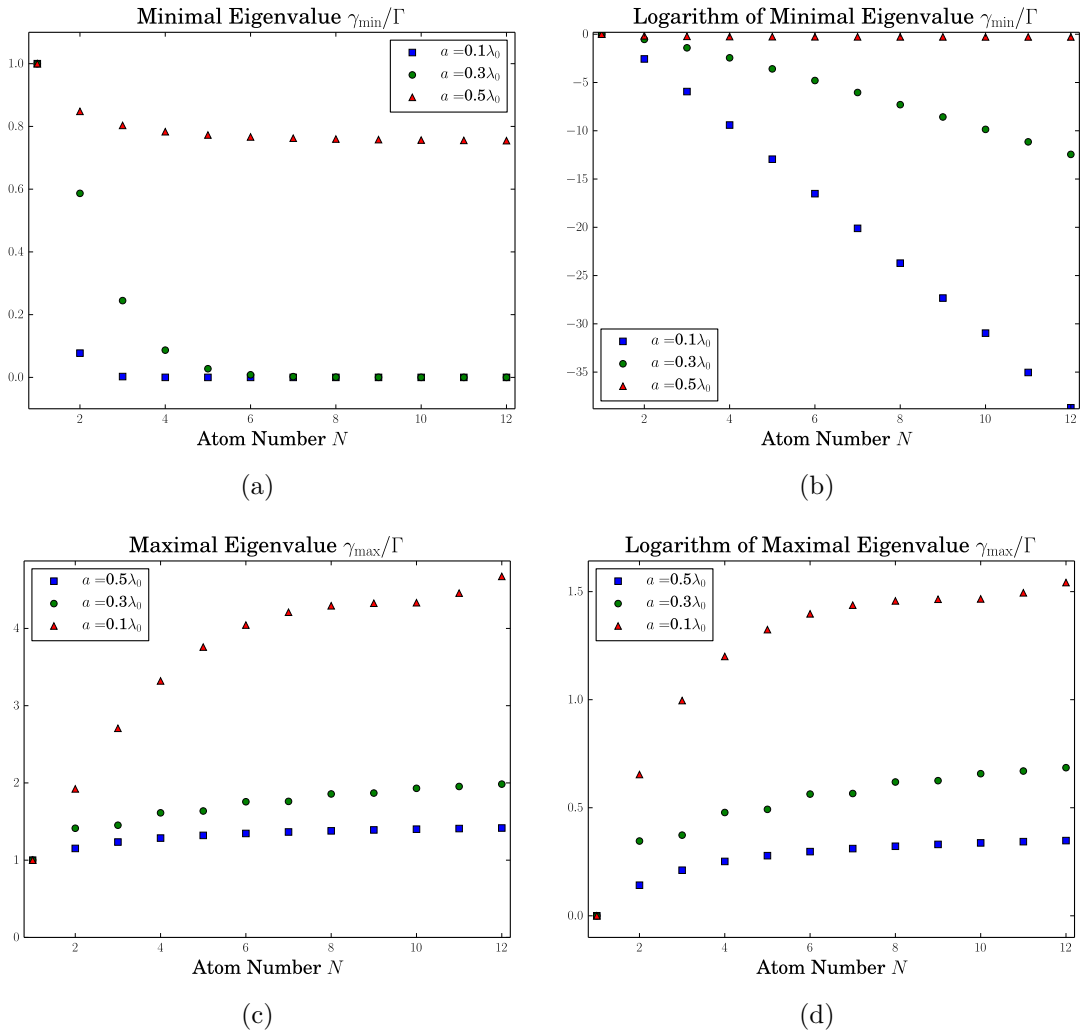

Figure 2.3: *Scaling of minimal and maximal eigenvalue.* The graphs present the scaling of the minimal and maximal eigenvalues of the decay rate matrix, $\gamma_{\min}$ and $\gamma_{\max}$ in units of the single atom decay rate Γ, with the atom number N. (a) and (c) show the real scaling of minimum and maximum, respectively. It already becomes clear that the minimum decreases way faster than the maximum grows. (c) and (d) show the logarithmic scaling where one can see that while the minimum decreases exponentially (linear in logarithmic plot), the maximum grows only polynomially with N.

2.2.5 Scaling of Decay Rates in a Realistic System

Considering only the eigenvalues of the decay rate matrix is not quite realistic since it does not account for effects like coherent population redistribution between the atoms due to dipole-dipole interaction. This can lead to an increase of the minimally possible decay rate of the eigenstates of the system, i.e. of the Hamiltonian defined in (2.7).

An approximate yet more realistic method of estimating the minimal decay rate is to initialize the system in the fully inverted state and letting it decay freely, explicitly including dipole-dipole interaction. During this time evolution one can measure the population of the ground state. Obviously, the states of larger decay rates decay faster. Hence, when considering sufficiently large times all populations but the state of lowest decay rate $\gamma_{\min}$ (and the ground state) can be neglected. The ground state population evolves in time as depicted in Fig. 2.4 and for large times can be safely approximated as

$$p_G(t) \approx 1 - e^{-\gamma_{\min} t}, \quad \text{for} \quad t \approx \gamma_{\min}^{-1}. \tag{2.22}$$

It is then possible to fit this presumed form of the ground state population. However, it

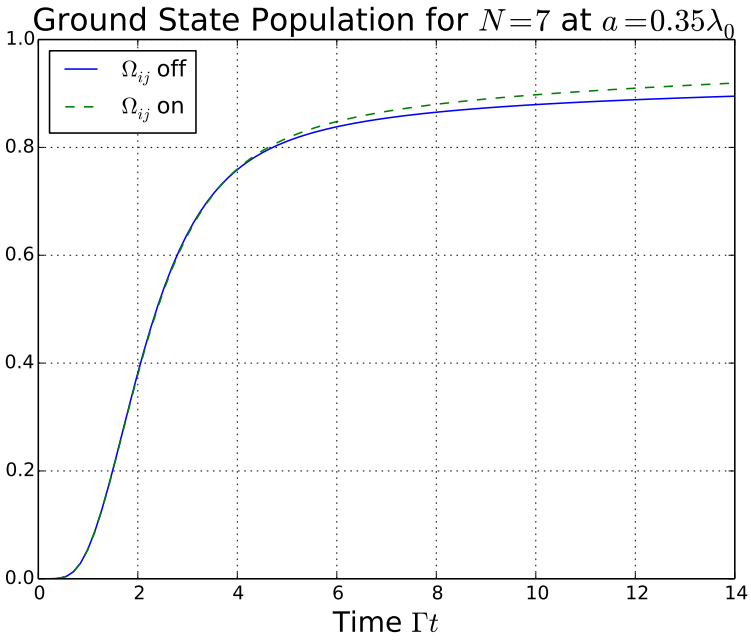

Figure 2.4: *Ground state population as a function of time.* Presented is the population of the ground state of a chain of $N = 7$ atoms at a distance of $a = 0.35\lambda_0$. It becomes clear that the decay is enhanced if dipole interaction is included, i.e. the ground state population grows faster in time if Ω_{ij} is taken into account as well. The single atom decay rate Γ has been chosen to be unity, yielding a unitless time.

is convenient to fit to the logarithm of this approximate function since that will simply yield a linear dependence instead of an exponential one. The decay rates obtained via this method are displayed in Fig. 2.5. Though larger than the minimal eigenvalue the scaling essentially remains the same, i.e. exponential in N, which becomes clear when comparing Fig. 2.3(b) and 2.5(b).

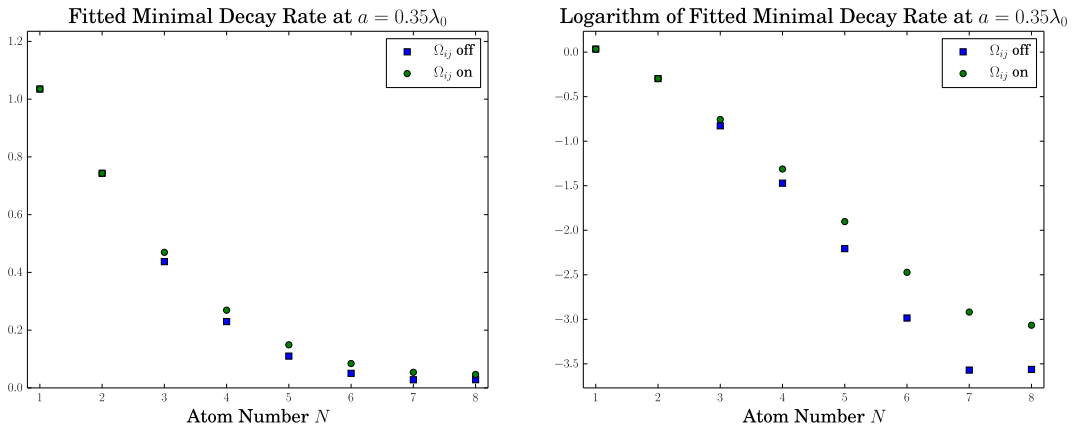

(a) (b)

Figure 2.5: *Scaling of the fitted minimal decay rate with the atom number.* The decay rates have been fitted according to (2.22) for different atom numbers N at a distance of $a = 0.35\lambda_0$. It is again clear that the dipole-dipole interaction has the unfavourable effect of enhancing the decay rate. Still, as it can be seen in (b) the minimal decay rate exhibits an exponential decrease (or at least close to it) in N. Unfortunately, numerical methods are limited to small atom numbers since the computation of the full time evolution requires solving a set of 4^N coupled differential equations.

2.3 Reduction of Decay

For a vast field of applications, some of which will be presented in this very thesis, it is of interest to reduce the decay of an ensemble of two-level atoms. Some examples for such applications are quantum memory, increasing the lifetime of entanglement, an enhancement of quantum metrology (See chapter 3), etc. The simplest theoretical and also experimental treatment of such an ensemble is, however, addressing all particles in the ensemble in the same way. This will in all cases lead to a collective state in the symmetric subspace, as mentioned before. Unfortunately, such states are usually super-radiant, meaning that not only is the decay not reduced by interaction of the atoms, but rather even vastly enhanced. Obviously, such an enhanced decay is unfavourable for a lot of applications and for everything that will be treated in this thesis.
In order to address collective states of low symmetry one has to manipulate each atom in the ensemble individually, which already poses a problem for an exact theoretical treatment, but definitely presents a challenge in terms of experimental realizability. However, as the theoretical and numerical results will show, the effects of super-radiance can not only be eliminated but even reversed, effectively utilizing collective effects to achieve vastly lower collective decay. States with such a reduced decay rate will be dubbed *sub-radiant*. Furthermore, it will be shown that this reduced rate of decay is decreased even further when adding more atoms to the chain.

2.3.1 Phase Distribution

The physical idea behind this reduction of decay is to make use of the interaction between particles. Specifically, instead of keeping all atoms in phase, as is the case for super-radiance (symmetric states), one aims to equally spread the phases in order for them to minimize the symmetry of the state (See Fig. 2.6). Another way to think of

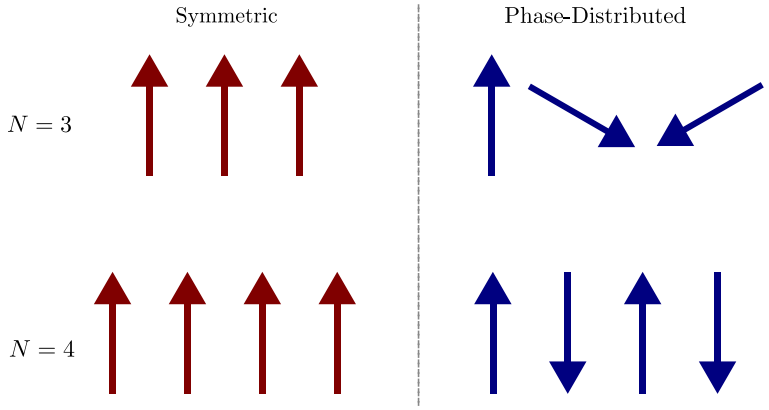

Figure 2.6: *Schematics of phase distribution.* The symmetric and phase-distributed case for a chain of $N = 3$ and $N = 4$.

this minimization of symmetry is that highest asymmetry causes maximally destructive interference upon emission, i.e. less photons are emitted and the decay rate is therefore lower. Mathematically, one can further motivate this idea by trying to find a state which minimizes the overlap with super-radiant states.

$$|\psi_\phi\rangle = \frac{1}{\sqrt{2^N}} \bigotimes_{j=1}^{N} (|g\rangle + e^{i\phi(j-1)} |e\rangle) \tag{2.23}$$

Unfortunately, analytical investigation is already terminated at this point. However, one can gain more insight when working in a subspace of the system restricted to only a single excitation. Also, from a physical point of view, one could anticipate that the state of the system with the lowest possible decay rate contains a single excitation since states of that form can only decay to the ground state whilst states of higher excitations couple to a manifold of states enhancing their decay rate. Hence, for purposes of further investigation, it makes sense to work in this subspace. Note, however, that no actual proof that the state of lowest decay rate is in this subspace will be provided.

2.3.2 The Single-Excitation Subspace

The states of our system are also eigenstates of the collective operator S_z. Hence, such a state can only be a superposition of bare states (bare basis $\{|e\rangle, |g\rangle\}^{\otimes N}$) containing the same number of excitations. Therefore, the eigenbasis of the Hamiltonian can be split

into subsets of different excitation numbers. Each subset of states containing a certain amount of excitations forms a basis in the respective subspace. As it was mentioned before, however, the analytical form of those eigenstates is unknown, so one can only make use of states close to the eigenstates and of relevance for physical investigations. Specifically, we will be considering the subspace containing a single excitation (exciton) and approximate eigenstates in that space. The lifetime of such states has also been subject to recent research [12].
The symmetric state in the single-excitation subspace is assumed to be the symmetric Dicke state containing only one excitation, also referred to as the $|W\rangle$ state,

$$|W\rangle = \frac{1}{\sqrt{N}} \sum_{j=1}^{N} \sigma_j^+ |G\rangle \,. \tag{2.24}$$

The overlap with the phase-spread state (2.23), that one seeks to minimize, yields

$$\langle W|\psi_\phi\rangle = \frac{1}{N} \sum_{j=1}^{N} e^{i\phi(j-1)} \;\rightarrow\; 0. \tag{2.25}$$

Equation (2.25) is satisfied for phases distributed equally over 2π, namely of the form

$$\phi = \frac{2\pi m}{N}, \tag{2.26}$$

where m is an integer that counts the different possibilities of distributing the phases. When $m = 0$, the overlap in (2.25), is maximized instead of minimized, since this corresponds to a state of zero phases, i.e. the $|W\rangle$ state itself. The same is true for $m = N$. Therefore m is limited to $0 < m < N$ for the phase-spread state to fulfil (2.25).

Phase States

The phase states for different m form a basis in the single excitation subspace. Namely, the set of states $\{|m\rangle\}_{m=0}^{N-1}$, where

$$|m\rangle := \frac{1}{\sqrt{N}} \sum_{j=1}^{N} e^{-i\varphi_j^{(m)}} \sigma_j^+ |G\rangle \tag{2.27}$$

span the single-excitation Hilbert space of dimension N. The phases were redefined to include the index j, such that

$$\varphi_j^{(m)} = \frac{2\pi m}{N}(j-1). \tag{2.28}$$

With this definition of phases the phase states are obviously normalized. In order for them to form a basis, they have to be mutually orthogonal. This condition is also

fulfilled,

$$\begin{aligned}\langle m'|m\rangle &= \frac{1}{N}\sum_{j,k=1}^{N} e^{i(\varphi_k^{(m')}-\varphi_j^{(m)})}\langle G|\,\sigma_k^-\sigma_j^+\,|G\rangle = \frac{1}{N}\sum_{j,k=1}^{N} e^{i(\varphi_k^{(m')}-\varphi_j^{(m)})}\delta_{kj} \\ &= \frac{e^{i(m-m')}}{N}\sum_{j=1}^{N} e^{i\frac{2\pi}{N}j(m'-m)} = \delta_{mm'}. \end{aligned} \tag{2.29}$$

Note, that the state $|m=0\rangle$ is the previously used $|W\rangle$ state. Furthermore, it shall be stated at this point that the phase states are eigenstates of the collective operator S_z to one degenerate eigenvalue,

$$S_z\,|m\rangle = \left(-\frac{N}{2}+1\right)|m\rangle\,, \quad \forall\ m. \tag{2.30}$$

Hence, they are eigenstates of H_0, yet not of H_{dip} effectively making them no eigenstates of the system under consideration. However, they do share symmetry with, and therefore physical properties of, the actual eigenstates.
This point can be shown as follows: Considering the dipole-dipole interaction Ω_{ij} in a chain configuration of atoms at extremely small distances, it is sufficiently close that

$$\frac{\Omega_{i,i+2}}{\Omega_{i,i+1}} \to 0, \quad a \ll \lambda_0, \tag{2.31}$$

i.e. the interaction between nearest neighbours is dominant over long range interactions. Furthermore, one needs to assume N to be large in order to push the upper limit of the sum in (2.32) from $N-1$ to N. The dipole Hamiltonian when only considering interactions with the nearest left and right neighbour then can approximately be written as

$$H_{dip} \approx \Omega\sum_j\left(\sigma_j^+\sigma_{j+1}^- + \sigma_j^+\sigma_{j-1}^-\right) = \Omega\sum_{j=1}^{N}\left(\sigma_j^+\sigma_{j+1}^- + \sigma_{j+1}^+\sigma_j^-\right). \tag{2.32}$$

Here, $\Omega = \Omega_{j,j+1},\ \forall\ j$ is the strength of the dipole-dipole interaction between nearest neighbours. Note that the action of the operator σ_k^- on a phase state as defined in (2.27) is

$$\sigma_k^-\,|m\rangle = \frac{1}{\sqrt{N}}\sum_{j=1}^{N} e^{-i\varphi_j^{(m)}}\sigma_k^-\sigma_j^+\,|G\rangle = \frac{e^{-i\varphi_k^{(m)}}}{\sqrt{N}}. \tag{2.33}$$

Hence, the action of the dipole Hamiltonian in the approximate form in (2.32) on a phase state [6][13] is

$$\begin{aligned} H_{dip}\left|m\right\rangle &= \frac{\Omega}{\sqrt{N}}\sum_j (e^{-i\varphi_{j+1}^{(m)}}\sigma_j^+\left|G\right\rangle + e^{-i\varphi_j^{(m)}}\sigma_{j+1}^+\left|G\right\rangle) \\ &= \frac{\Omega}{\sqrt{N}}\sum_j (e^{-i\frac{2\pi m}{N}}e^{-i\varphi_j^{(m)}}\sigma_j^+\left|G\right\rangle + e^{i\frac{2\pi m}{N}}e^{-i\varphi_j^{(m)}}\sigma_{j+1}^+\left|G\right\rangle) \\ &= \Omega(e^{-i\frac{2\pi m}{N}}\left|m\right\rangle + e^{i\frac{2\pi m}{N}}\left|m\right\rangle) = 2\Omega\cos\frac{2\pi m}{N}\left|m\right\rangle. \end{aligned} \tag{2.34}$$

From this it becomes clear, that even though the phase states are not eigenstates of the system, they are indeed very close to them when working in a chain configuration with small distances between the atoms. It is therefore of interest to investigate the decay of these states.

Decay of the Phase States

In order to find the decay rate of a state one has to consider the master equation (2.13). The decay rate is the rate at which the population of state $\left|m\right\rangle$, namely the density matrix element ρ_{mm}, decreases over time. Given the complete density matrix $\rho = \sum_{m,m'=0}^{N-1}\rho_{mm'}\left|m\right\rangle\left\langle m'\right|$ which obeys the master equation, the differential equation for the element ρ_{mm} is

$$\dot{\rho}_{mm} = \left\langle m\right|\dot{\rho}\left|m\right\rangle = i\left\langle m\right|[\rho, H]\left|m\right\rangle + \left\langle m\right|\mathcal{L}[\rho]\left|m\right\rangle. \tag{2.35}$$

In order to keep complexity to a minimum, it makes sense to consider (2.35) term by term. First, using (2.33), the commutator yields

$$\begin{aligned} i\left\langle m\right|[\rho, H]\left|m\right\rangle &= i\left\langle m\right|[\rho, H_{dip}]\left|m\right\rangle \\ &= \frac{i}{N}\sum_{m',j\neq k}\Omega_{jk}\left(\rho_{mm'}e^{i(\varphi_j^{(m')}-\varphi_k^{(m)})} - \rho_{m'm}e^{-i(\varphi_j^{(m')}-\varphi_k^{(m)})}\right) \\ &= -\frac{1}{N}\sum_{m',j\neq k}2\Omega_{jk}\mathrm{Im}\{\rho_{mm'}e^{i(\varphi_j^{(m')}-\varphi_k^{(m)})}\}. \end{aligned} \tag{2.36}$$

Furthermore, it is clear that the overlap of the first term of the used Lindblad operator does not conserve excitation and hence is zero for all phase states (as they reside in the single-excitation manifold).

$$\sum_{\substack{j,k\\ \tilde{m},\tilde{m}'}}\Gamma_{jk}\left\langle m\right|\sigma_j^-\rho_{\tilde{m}\tilde{m}'}\left|\tilde{m}\right\rangle\left\langle\tilde{m}'\right|\sigma_k^+\left|m'\right\rangle = 0, \quad \forall\ m, m' \tag{2.37}$$

The remaining terms in the Liouvillian, however, do couple a state in the single-excitation manifold to others. It is easy to see that

$$\begin{aligned}\langle m|\,\mathcal{L}[\rho]\,|m\rangle &= -\sum_{j,k}\frac{\Gamma_{jk}}{2}\left(\langle m|\,\sigma_j^+\sigma_k^-\rho\,|m\rangle + \langle m|\,\rho\sigma_j^+\sigma_k^-\,|m\rangle\right)\\ &= -\sum_{j,k}\Gamma_{jk}\mathrm{Re}\{\langle m|\,\sigma_j^+\sigma_k^-\rho\,|m\rangle\}.\end{aligned} \tag{2.38}$$

Hence, one only needs to compute one overlap in order to find the action of the Liouville operator,

$$\begin{aligned}\sum_{j,k}\Gamma_{jk}\,\langle m|\,\sigma_j^+\sigma_k^-\rho\,|m\rangle &= \sum_{m',j,k}\Gamma_{jk}\rho_{m'm}\,\langle m|\,\sigma_j^+\sigma_k^-\,|m'\rangle =\\ &= \sum_{m',j,k}\Gamma_{jk}\rho_{m'm}e^{i(\varphi_j^{(m)}-\varphi_k^{(m')})}.\end{aligned} \tag{2.39}$$

So, the master equation yields the following differential equation for the population of a phase state $|m\rangle$,

$$\dot{\rho}_{mm} = -\frac{1}{N}\sum_{m'}\left(\sum_{j\neq k}2\Omega_{jk}\mathrm{Im}\{\rho_{mm'}e^{i(\varphi_j^{(m')}-\varphi_k^{(m)})}\} + \sum_{j,k}\Gamma_{jk}\mathrm{Re}\{\rho_{mm'}e^{i(\varphi_j^{(m')}-\varphi_k^{(m)})}\}\right). \tag{2.40}$$

In order to find the decay rate of ρ_{mm} one would have to solve this equation, which is not possible analytically. However, making the drastic move of discarding all terms where $m' \neq m$, equation (2.40) can be investigated analytically. This part of the differential equation corresponds to decay directly to the ground state, effectively neglecting all coherences to other states $\rho_{mm'}$. When working in the single-excitation subspace, the states can only decay directly to the ground state. Hence, the idea to gain physical insight by investigating this part of the differential equation only is justified.
By discarding all terms where $m' \neq m$, equation (2.40) is reduced to its homogeneous part, yielding

$$\dot{\rho}_{mm}^{hom} = -\frac{\rho_{mm}^{hom}}{N}\left(\sum_{j\neq k}2i\Omega_{jk}\sin\left(\varphi_j^{(m)}-\varphi_k^{(m)}\right) + \sum_{j,k}\Gamma_{jk}\cos\left(\varphi_j^{(m)}-\varphi_k^{(m)}\right)\right) = -\gamma_m\rho_{mm}^{hom}. \tag{2.41}$$

This differential equation can readily be solved by $\rho_{mm}^{hom} = \rho_{mm}^{hom}(0)e^{-\gamma_m t}$, hence the population decays with the rate γ_m. The expression for this rate has been implicitly

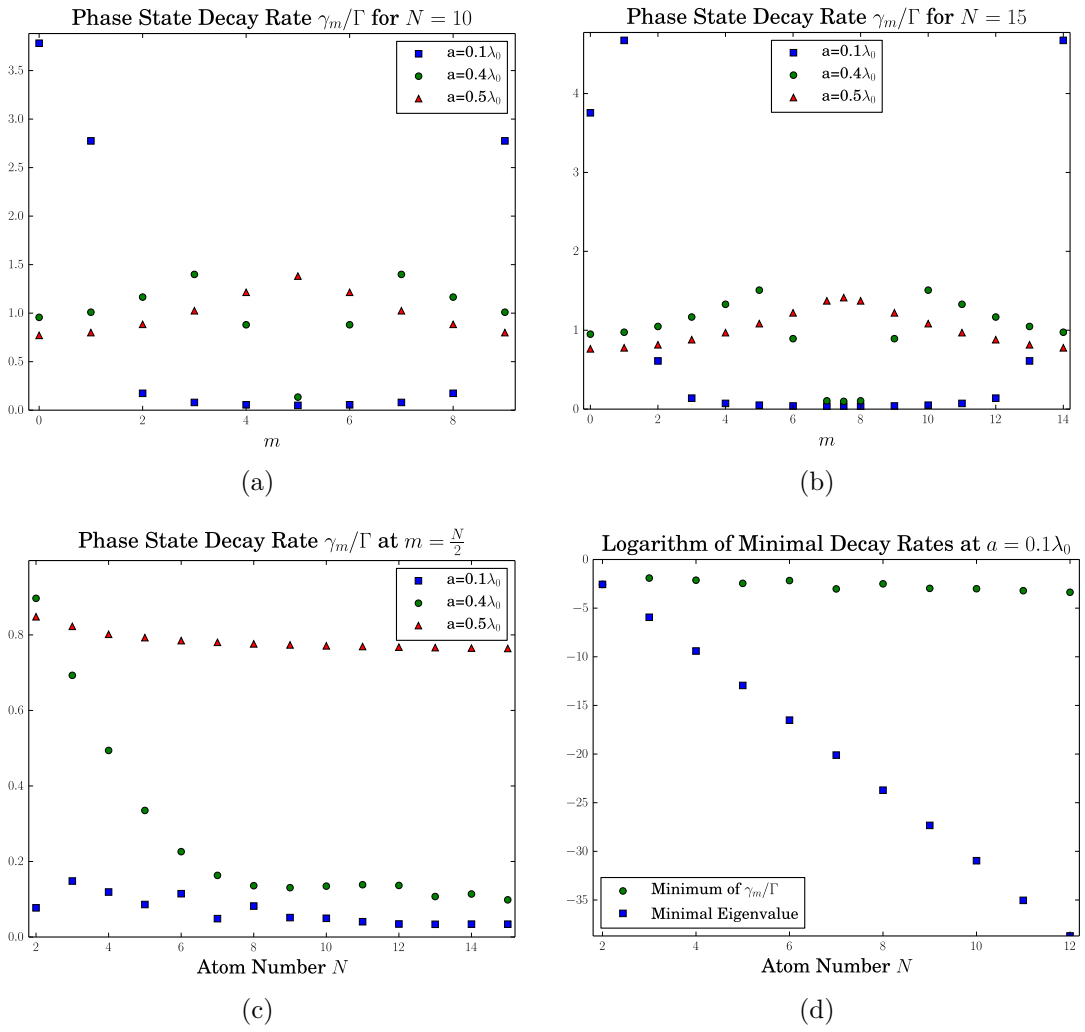

Figure 2.7: *Scaling of the phase state decay rate with m at different distances.* (a) and (b) show the decay rate γ_m/Γ as a function of m at different distances. As expected, for distances where the mutual decay rates between nearest neighbour atoms are positive, the minima lie at $m = \frac{N}{2}$, while if the mutual coupling between closest atoms is negative, $m = 0$ becomes optimal. Furthermore, it is clear from (b) that for a large number of atoms, i.e. additional negative couplings between atoms farther apart, small values of m can enhance the decay rate instead of decreasing it.
In (c), on the other hand, the scaling of the phase state decay rate at $m = \frac{N}{2}$ with the atom number N is visible. As long as one is working in the area of positive nearest neighbour couplings, the decay rates appear to shrink with growing N. However, for distances where nearest neighbour couplings are negative (see $a = 0.5\lambda_0$), the scaling with N is becomes comparable to the maximal eigenvalue of the matrix $[\Gamma_{ij}]$ (See Fig. 2.3(c)). Finally, (d) shows the logarithm of the minimal decay rates, where it becomes clear that, even though slower, the scaling of the minimal phase state decay rate is still exponential with N.

defined in (2.41), but can be further simplified.

$$\begin{aligned}\gamma_m &= \frac{1}{N}\left(\sum_{j\neq k}\left(2i\Omega_{jk}\sin\left(\varphi_j^{(m)}-\varphi_k^{(m)}\right)+\Gamma_{jk}\cos\left(\varphi_j^{(m)}-\varphi_k^{(m)}\right)\right)+\sum_{j=1}^{N}\Gamma_{jj}\right)\\ &= \Gamma+\frac{1}{N}\left(\sum_{j<k}2i\Omega_{jk}(\sin\left(\varphi_j^{(m)}-\varphi_k^{(m)}\right)+\sin\left(\varphi_k^{(m)}-\varphi_j^{(m)}\right))+\sum_{j\neq k}\Gamma_{jk}\cos\left(\varphi_j^{(m)}-\varphi_k^{(m)}\right)\right)\\ &= \Gamma+\frac{1}{N}\sum_{j\neq k}\Gamma_{jk}\cos\left(\varphi_j^{(m)}-\varphi_k^{(m)}\right) \qquad (2.42)\end{aligned}$$

Using the exact definition of the phases (2.28), one can gain a quite simple expression for the phase state decay rate, i.e.

$$\gamma_m = \Gamma+\frac{1}{N}\sum_{j\neq k}\Gamma_{jk}\cos\frac{2\pi m}{N}(j-k), \qquad (2.43)$$

making an analytical analysis possible (See also [14][15]). Since especially the minimal and maximal decay rates are of interest, one seeks to extremize the decay rate with respect to m. This can be done by taking the derivative of (2.43),

$$\begin{aligned}&\frac{\partial\gamma_m}{\partial m} = -\frac{1}{N}\sum_{j\neq k}\Gamma_{jk}\frac{2\pi}{N}(j-k)\sin\frac{2\pi m}{N}(j-k)=0,\\ &\Leftrightarrow\quad \frac{2\pi m}{N}(j-k)=n\pi,\quad n\in\mathbb{Z}. \qquad (2.44)\end{aligned}$$

Note, that this extremization condition is only with respect to m. The global extremes of the decay rate, however, still depend on the size of the lattice constant a, i.e. on the specific values of Γ_{jk} for different j,k. Since these mutual decay rates can be positive or negative depending on the interatomic distance, the global extremes are not necessarily identical to the local extremes given by an m that satisfies the condition in (2.44). However, one can consider certain distances where the global and local extremes coincide. One example of such a distance is the limit of very small lattice constants ($a<0.5\lambda_0$), since this restriction corresponds to a majority of positive mutual decay rates Γ_{jk} (See Fig. 2.1).
Obviously, $m=0$ satisfies the condition in (2.44). This choice of m corresponds to the local maximum of γ_m, as it is expected since the state $|m=0\rangle$ is super-radiant. If $m>0$, then

$$\frac{2\pi m}{N}=n\pi \quad\Leftrightarrow\quad m=\frac{N}{2}. \qquad (2.45)$$

Choosing m in such a way will yield a local minimum for small distances between the atoms in a chain, yet can result in a maximum if the distance between the atoms is

chosen in such a way that the majority of the mutual decay rates is negative. Since the mutual decay rates in a chain configuration change sign at a distance of about $a \approx 0.5\lambda_0$ (See Fig. 2.1), one can anticipate the transition to the case where $m = 0$ is optimal to occur in this region. This is illustrated in Fig. 2.7(a). Note also, that for odd numbers of atoms, the extremizing m is no longer an integer but a half-integer. Even though the state that corresponds to this value of $m = \frac{N}{2}$ is not an element of the phase state basis $\{|m\rangle\}$ for odd N, it is still a valid state in this subspace. The function of the decay rate will yield two identical local extremes when investigated for integer m only in the case of an odd atom number N at $m = \frac{N\pm1}{2}$. However, the one true local extreme is of course at $m = \frac{N}{2}$.
Numerical results of decay rates for different m can be seen in Fig. 2.7 and validate every point in the above discussion.

Dipole Shifts of the Phase States

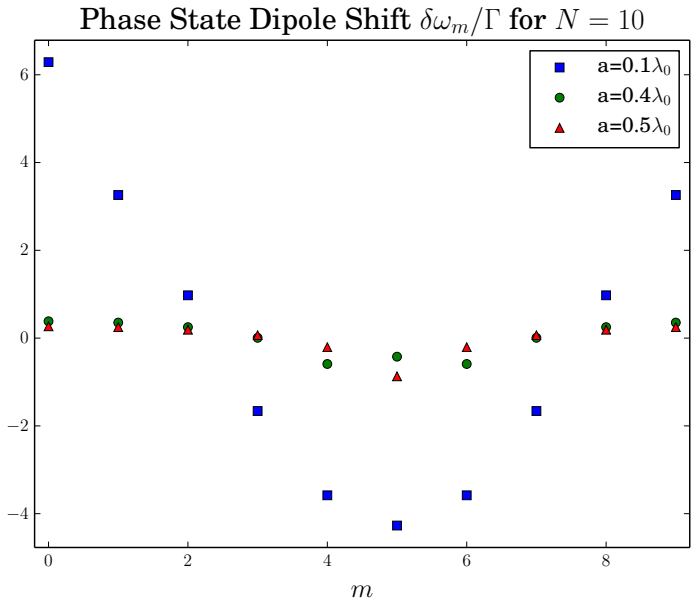

Figure 2.8: *Dipole shifts for different m.* As opposed to the decay rates (See Fig. 2.7), for a distance of $a = 0.5\lambda_0$ the minimum still remains at $m = \frac{N}{2}$. This is due to the fact that the mutual dipole-dipole interaction remains positive for this distance (See Fig. 2.1). However, at distance $a = 0.4\lambda_0$, the minimum is not where it would be expected. This is again caused by the specific form of the Ω_{ij} and unfortunate sign change of negative parts of the function at larger distances (next-nearest neighbour and farther). The results of minimization hold, though, when restricting the investigation to very small distances in the chain ($a \approx 0.1\lambda_0$).

It is of further interest to investigate the dipole shifts of the phase states. The energy

shift $\Delta\omega_m$ of a state $|m\rangle$ that is caused by the dipole Hamiltonian H_{dip} can be computed by

$$\begin{aligned}\Delta\omega_m &= \langle m| H_{dip} |m\rangle = \sum_{j\neq k} \Omega_{jk} \langle m| \sigma_j^+ \sigma_k^- |m\rangle \\ &= \sum_{j\neq k} \frac{\Omega_{jk}}{N} e^{i(\varphi_j^{(m)} - \varphi_k^{(m)})} = \frac{1}{N} \sum_{j\neq k} \Omega_{jk} \cos \frac{2\pi m}{N}(j-k). \end{aligned} \tag{2.46}$$

The relation in (2.33) was once again used for this calculation. The similarity of the function for the dipole shift $\Delta\omega_m$ in (2.46) to the computation of the decay rate γ_m in (2.43) is obvious. Therefore, extremization of (2.46) does not have to be performed since it obviously yields the same result as for γ_m (see (2.44)). Hence, the state of lowest decay rate $|m = \frac{N}{2}\rangle$ (at small distances in the chain) is also subject to the minimal dipole shift. Note that the dipole shifts, as opposed to the decay rate, can be negative. The minimal dipole shift is therefore the maximally negative one. The dipole shifts for different states $|m\rangle$ have been plotted in Fig. 2.8.

In conclusion, it is again noteworthy that these phase states are of great physical relevance when discussing collective effects of decay in an ensemble of two-level emitters containing one excitation only. This is due to their symmetry properties, which are quite similar to the properties exhibited by eigenstates of the system, even though the states are not identical. This motivates further investigation of such phase-distributed states and their applications on realistic systems, including more than one excitation.

2.4 Rotations on the Bloch Sphere

The state of an ensemble of two-level quantum systems can be described by a Bloch vector. Said vector is the expectation value of the total spin operator $\boldsymbol{S} = (S_x, S_y, S_z)$. The set of all Bloch vectors spans a three-dimensional sphere with a diameter of length N, the Bloch sphere. A change of the state of an ensemble, e.g. by applying an exciting laser, is mathematically equivalent to a rotation of the Bloch vector on the Bloch sphere.

2.4.1 General Rotations on the Bloch Sphere

The Pauli matrices are generators of three-dimensional rotations. A rotation of the Bloch vector of a single particle around an angle ϕ therefore is just $e^{i\frac{\phi}{2}\sigma_\nu}$, when rotated about the axis $\nu \in \{x, y, z\}$. This can be generalized to describe rotations of the collective Bloch vector, namely

$$R_\nu[\phi] = \prod_{j=1}^{N} e^{i\frac{\phi}{2}\sigma_\nu^{(j)}}. \tag{2.47}$$

The operators $\sigma_\nu^{(j)}$ act on the j-th particle non-trivially, as in (2.4). Rotations of the form (2.47) rotate each single particle Bloch vector around the same angle ϕ. This corresponds to an addressing of all atoms in the same way effectively working on the symmetric subspace. This also leaves the length of the collective Bloch vector invariant. Note also, that when working with rotations on the Bloch sphere, it is assumed that the excitation of the atoms is instant, i.e. there is no time for transitions (decay) to take place.
The definition in (2.47) can, however, be extended to rotations which address each particle individually, simply by replacing the angle ϕ by a set of distinct angles $\{\phi_j\}_{j=1}^N$, rotating each single particle Bloch vector around an arbitrary angle. Such an individual addressing is necessary in order to change the symmetry of a state.

2.4.2 Phase-Spread Rotations

It was mentioned before that states of lower symmetry appear to decay more slowly. An example of such low symmetry states was given by the phase states (2.23). However, the system has first to be prepared in such a state or at least in a state close to it. The aim now is to formulate so-called phase-spread rotations which can be applied to an arbitrary state and achieve the goal of putting the system in a state close to the phase states. This is possible and hence gives rise to the hope that one can reduce the decay of the system by the application of such rotations.
The aim is to reduce the symmetry by manipulating the individual phases of the atoms in the chain while leaving the state otherwise invariant, i.e. the number of excitations in the state remains unchanged. Since the single atom states are eigenstates of the Pauli matrix σ_z, such a manipulation of phases can be achieved by phase-spread rotations about the z-axis

$$R_z^{(m)} = \prod_{j=1}^{N} e^{i\varphi_j^{(m)}\sigma_z^{(j)}/2}. \tag{2.48}$$

Here, the equally spread phases $\varphi_j^{(m)}$ as defined in (2.28) were used. The integer m again simply counts the possibilities of equally distributing N phases over 2π. Note that, due to symmetry of the rotations in m, it is sufficient to consider the range where $0 \leq m \leq \lfloor \frac{N}{2} \rfloor$, where $\lfloor \frac{N}{2} \rfloor$ is the largest integer smaller or equal to $\frac{N}{2}$.
For states that have a Bloch vector with some extension in the x-y-plane, application of a phase-spread rotation as in (2.48) will have the effect of equally spreading these x- and y-components about the z-axis such that they add up to zero, yielding a state with a Bloch vector aligned with the z-axis.

Two Atom Case

To further motivate the application of such phase-spread rotations, it is of use to investigate the case of $N = 2$. Two bases can be chosen, the bare basis $\{|gg\rangle, |ge\rangle, |eg\rangle, |ee\rangle\}$

and the collective basis $\{|G\rangle, |S\rangle, |A\rangle, |E\rangle\}$. These two bases are connected by

$$|G\rangle = |gg\rangle, \quad |S\rangle = \frac{1}{\sqrt{2}}(|eg\rangle + |ge\rangle),$$
$$|E\rangle = |ee\rangle, \quad |A\rangle = \frac{1}{\sqrt{2}}(|eg\rangle - |ge\rangle). \tag{2.49}$$

The states $|S\rangle$ and $|A\rangle$ are commonly referred to as the symmetric and asymmetric state, respectively. Note that, the collective basis is the actual eigenbasis of the Hamiltonian as defined in (2.7) and also coincides with the Dicke states for $N = 2$. Hence, it is most useful to work in this basis. Furthermore, it is noteworthy that the states in the single-excitation subspace, i.e. $|S\rangle$ and $|A\rangle$, are just the phase-states as defined in (2.27), with $|S\rangle = |m = 0\rangle$ and $|A\rangle = |m = 1\rangle$. Both these properties are a particularity of the two atom case.
Defining the mutual decay rates to be $\Gamma_{11} = \Gamma_{22} = \Gamma$ and $\Gamma_{12} = \Gamma_{21} = \gamma$, the system can decay through two decay channels with respective decay rates of $\gamma_S = \Gamma + \gamma$ and $\gamma_A = \Gamma - \gamma$. When computing the decay rates as shown in (2.43), it is easy to see that the symmetric decay rate γ_S corresponds to the symmetric state, while the asymmetric state decays with γ_A. When working in areas of small distances between the two atoms ($a < 0.5\lambda_0$), the asymmetric decay rate is significantly lower than the symmetric one.
The choice of m in the phase-spread rotations is obviously limited to be $m = 1$, yielding phases of $\varphi_1^{(1)} = 0$ and $\varphi_2^{(1)} = \pi$. These phases also lead to the property that $R_z^{(1)} = -\left(R_z^{(1)}\right)^{-1}$. Since both the ground state $|G\rangle$ and the fully inverted state $|E\rangle$ are invariant under rotations about the z-axis (up to negligible global phases), the only action of the phase-spread rotations will be on symmetric and asymmetric state.

$$R_z^{(1)}|S\rangle = \frac{1}{\sqrt{2}}\left(e^{-i\frac{\pi}{2}}|eg\rangle + e^{i\frac{\pi}{2}}|ge\rangle\right) = -i|A\rangle \tag{2.50}$$
$$R_z^{(1)}|A\rangle = -i|S\rangle \tag{2.51}$$

The global phase is, of course, of no relevance for the dynamics of the system. Hence, when given a state that is a superposition including the symmetric state, one can reduce its decay rate by applying such a phase-spread rotation. This application will effectively change the contribution of the symmetric state to the decay, that is γ_S, to the (eventually vastly) lower decay rate γ_A. This motivates the idea that one can also use the phase-spread rotations in order to reduce the decay in larger systems of high symmetry.

Chapter 3

Protected State Ramsey Spectroscopy

A well known procedure that is routinely performed on an ensemble of two-level atoms is the so-called Ramsey spectroscopy. The aim is to find the resonance frequency ω_0 of the addressed transition of the atoms in the ensemble with optimal precision. Due to the fact that the procedure includes an as long as possible period of free time evolution of the atoms, decay and collective effects are of great relevance. As it will be seen shortly, the mutual decay of such a system is a limiting factor in the measurment precision. It is therefore of interest to reduce said decay to a minimum. When performing Ramsey Spectroscopy, the common method is to address all atoms in the same way, effectively working on the symmetric (super-radiant) subspace of the system. This motivates the idea that not only one could eliminate the effect of super-radiance, but even exploit collective effects using phase-spread operations as discussed in Sec. 2.3. It will be shown that one can indeed utilize the phase-spread operations leading to a significant gain in the sensitivity when compared to the common procedure of Ramsey spectroscopy [4].

3.1 Ramsey Procedure

The standard Ramsey Procedure consists of three parts. With the ensemble initially being in the ground state, the first step is to apply a $\frac{\pi}{2}$-pulse, which corresponds to a rotation as defined in (2.47),

$$R_y\left[\frac{\pi}{2}\right] = \prod_{j=1}^{N} e^{i\frac{\pi}{4}\sigma_y^{(j)}} = e^{i\frac{\pi}{2}S_y}. \tag{3.1}$$

The application of this rotation to the ground state yields an initial state of the form

$$R_y\left[\frac{\pi}{2}\right]|G\rangle = \left(\frac{|e\rangle + |g\rangle}{\sqrt{2}}\right)^{\otimes N} = \frac{1}{\sqrt{2^N}} \sum_{k=0}^{N} \binom{N}{k}^{\frac{1}{2}} |\frac{N}{2}, -\frac{N}{2} + k\rangle\,. \tag{3.2}$$

Note that the first equality is the representation in the bare basis using single atom states $|e\rangle$ and $|g\rangle$, while the second is the representation of the state as a superposition

of symmetric Dicke states (collective states) $|S, M\rangle$. After the preparation of this state the system is subject to free time evolution and therefore to decay for a certain time τ. Then a second $\frac{\pi}{2}$-pulse is applied, rotating the system into a state close to the fully inverted state $|E\rangle = |e\rangle^{\otimes N}$ (See Fig. 3.1).

After the entire procedure the state inversion of the system, namely $\langle S_z \rangle$, is measured.

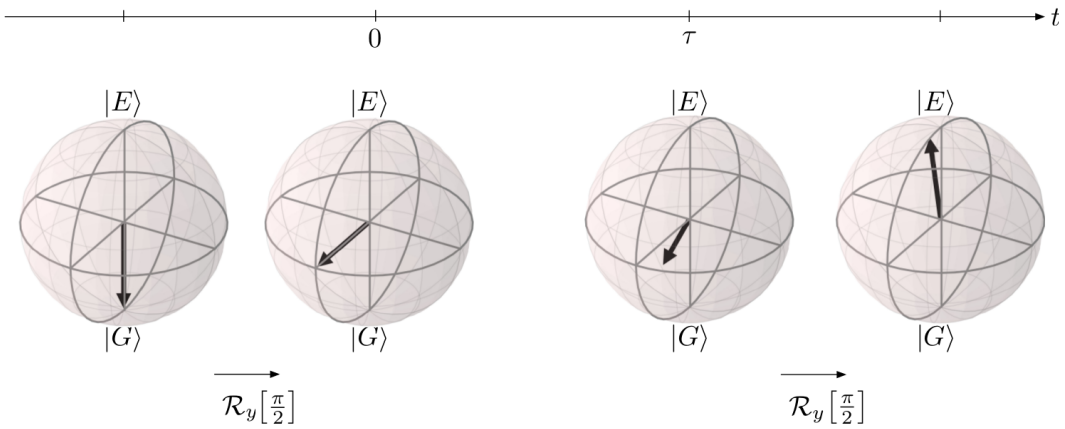

Figure 3.1: *Standard Ramsey Procedure.* The first $\frac{\pi}{2}$-pulse is applied instantaneously, such that the system is in a state with a Bloch vector perfectly aligned with the x-axis at time $t = 0$. This is followed by free time evolution until $t = \tau$, and finally a second $\frac{\pi}{2}$-pulse is applied.

Such a signal is shown in Fig. 3.2 as a function of the detuning $\omega = \omega_0 - \omega_l$, where ω_l is the reference frequency. Signal analysis, namely investigation of the slope of this function gives rise to the minimal signal sensitivity, $\delta\omega$, which is

$$\delta\omega = \min\left[\frac{\Delta S_z(\omega, \tau)}{|\partial_\omega \langle S_z \rangle(\omega, \tau)|}\right]. \tag{3.3}$$

Here, $\Delta S_z = \sqrt{\langle S_z^2 \rangle - \langle S_z \rangle^2}$ is the variance of S_z. The minimization is performed with respect to ω.

Since the system is in a superposition of all symmetric states (3.2), it is clear that the decay rate of the ensemble will be enhanced by collective effects (super-radiance). Even when ignoring all interactions and treating the atoms as independent, the signal sensitivity is vastly limited by the decay rate Γ,

$$\delta\omega_{ind} = \frac{e^{\Gamma\tau/2}}{\sqrt{N\tau}}. \tag{3.4}$$

It is clear that due to the simplified treatment this expression is not correct but provides a lower boundary for the common Ramsey procedure, since super-radiance will further limit the resolution to larger values than given by independent treatment. This, of

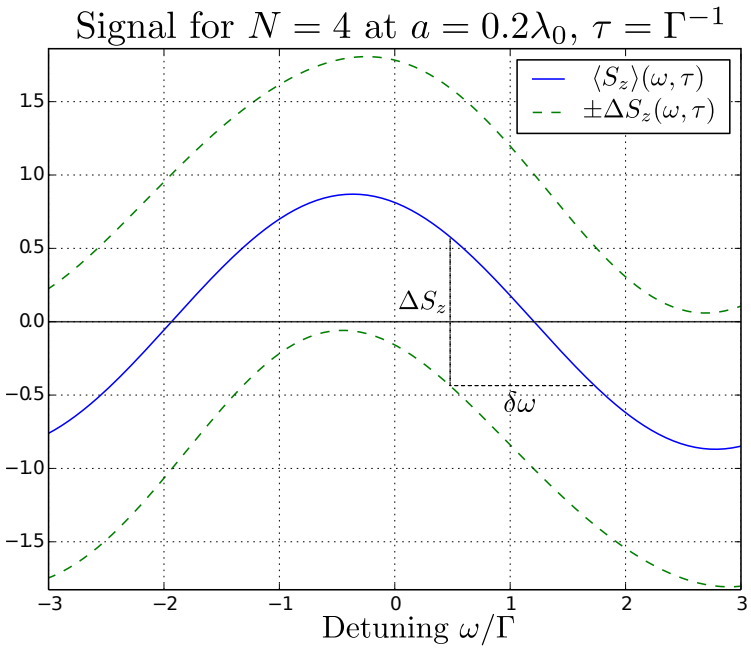

Figure 3.2: *Signal as a function of the detuning between the atomic transition and the excitation frequency.*

course, is again only for positive coupling between the atoms, i.e. positive Γ_{ij}. Hence, when working in a chain configuration, it is again of use to work with the restriction to small distances between nearest neighbour atoms. Furthermore it is noteworthy that the independent signal sensitivity is minimal at $\tau_{opt} = 2/\Gamma$.

3.2 Enhancement via State Protection

The basic idea now is to apply the rotations as defined in (2.48) in order to protect the system from decay during the free time evolution thereby retaining a state that is closer to the initally prepared one. The aim is to achieve a better signal sensitivity than when performing the common Ramsey technique.
A procedure similar to the one shown in Fig. 3.1 can be performed, which will include an additional rotation that will reduce the symmetry of the system. Namely, after the initial $\frac{\pi}{2}$-pulse, a phase-spread rotation will be applied, resulting in a state with zero average classical dipole (See Fig. 3.3).

$$R_z^{(m)} R_y \left[\frac{\pi}{2}\right] |G\rangle = \prod_{j=1}^{N} e^{i\varphi_j^{(m)} \sigma_z^{(j)}} \left(\frac{|g\rangle + |e\rangle}{\sqrt{2}}\right)^{\otimes N} \tag{3.5}$$

This pulse can loosely be dubbed *Generalized Ramsey Pulse*. The phases, once again, are $\varphi_j^{(m)} = \frac{2\pi m}{N}(j-1)$ with $0 < m < \lfloor \frac{N}{2} \rfloor$. As before, $\lfloor \frac{N}{2} \rfloor$ is the largest integer that is

smaller or equal to $\frac{N}{2}$. Unfortunately, there is no simple expression for states of this form. Analytical results are therefore fairly limited. In order to get to results that show the signal sensitivity, numerical methods will have to be applied.
After the free time evolution, the phase-spread must be reversed before the second $\frac{\pi}{2}$-pulse is being applied. Hence, instead of just applying $R_y\left[\frac{\pi}{2}\right]$ one has to apply $R_y\left[\frac{\pi}{2}\right](R_z^{(m)})^{-1}$, which can be referred to as the second generalized Ramsey pulse.

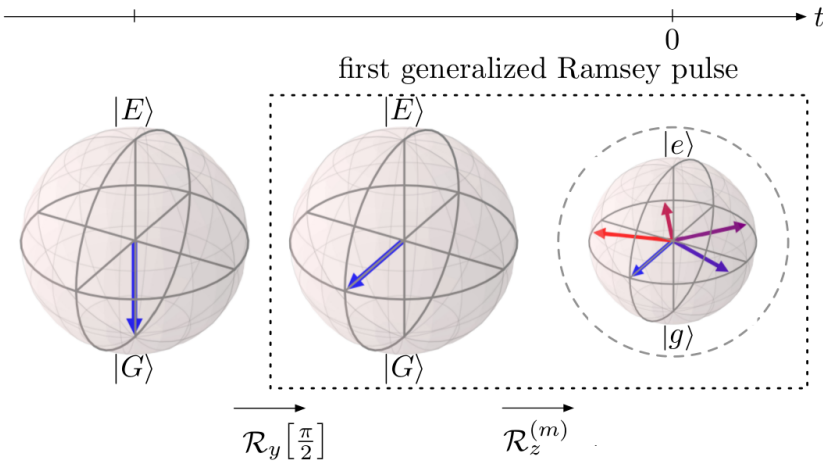

Figure 3.3: *Modified preparation step for Protected State Ramsey spectroscopy.*

3.3 Numerical Results

A full numerical simulation of Ramsey spectroscopy requires the computation of the free time evolution of the treated system and hence is numerically intense. Therefore numerical results will only be presented for small atom chains (See Fig. 3.5).
When comparing Fig. 3.5(a) and Fig. 3.5(b) (or Fig. 3.5(c) and Fig. 3.5(d)) it can be seen that the difference between the case where no phases are applied ($m = 0$) and the independent decay, but also their difference to the application of the optimal phase-spread rotations ($m = \frac{N}{2}$), are larger for smaller distances. This is due to the scaling of the collective effects with distance (See Fig. 2.1). Note also, that the enhancement achieved by applying optimal phase-spread rotations is also larger for more atoms (compare Fig. 3.5(a) and Fig. 3.5(b)). When recalling that the lowest possible decay rate of such a system scales most favourably in N (See Fig. 2.3(b)), and furthermore recounting the fact that one effectively reduces the system's decay by applying these phase-spread rotations, this effect of additional enhancement for larger atom numbers can be expected.
It was mentioned that the function of the signal sensitivity for independently decaying atoms possesses a minimum at $\tau_{opt} = 2/\Gamma$. The naive hope at this point is to use this

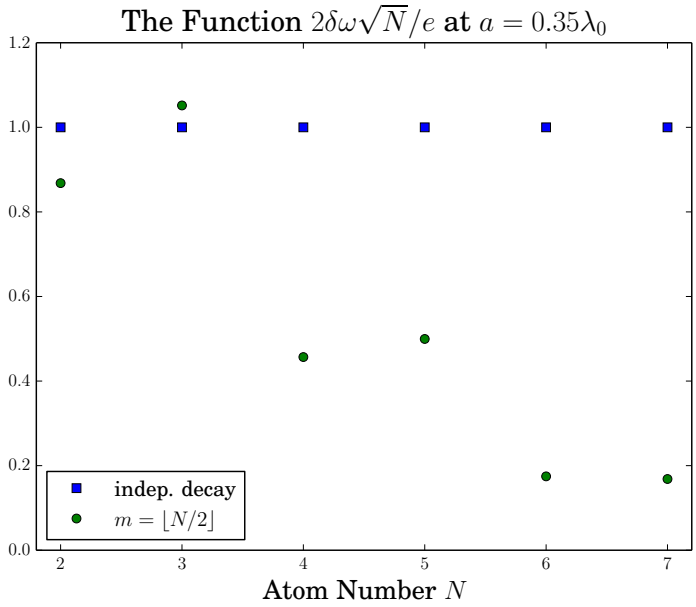

Figure 3.4: *Scaling of the optimal sensitivity with the atom number.* The minimal sensitivity (with respect to detuning and time) is plotted. It has been modified such that the scaling of the independent sensitivity from (3.4) ($\delta\omega_{ind} \propto 1/\sqrt{N}$) is rendered constant and normalized to unity (with $\Gamma = 1$). From this it is clear that the proposed method of Protected Ramsey spectroscopy yields a sensitivity that goes beyond the standard quantum limit.

in order to find the minimal decay rate of a system as treated in the Ramsey procedure and investigate its change with N, yielding a scaling similar to the minimal eigenvalue of the decay rate matrix. This will give some insight on the efficiency of the phase-spread rotations, namely how close one can get the system to the minimally possible rate of decay (see also Fig. 2.4). The decay rate will be computed as

$$\Gamma_{min} = \frac{2}{\tau_{opt}}. \tag{3.6}$$

The real result of interest is, however, shown in Fig. 3.4, where it is clearly shown that the scaling of the signal sensitivity with the atom number N gained via the proposed method of Ramsey spectroscopy goes beyond the scaling in the case of independently decaying atoms (3.4). As you can see in Fig. 3.6, the system is quite close to the minimal decay rate further justifying the application of phase-spread rotations and explaining the results shown in Fig. 3.5.

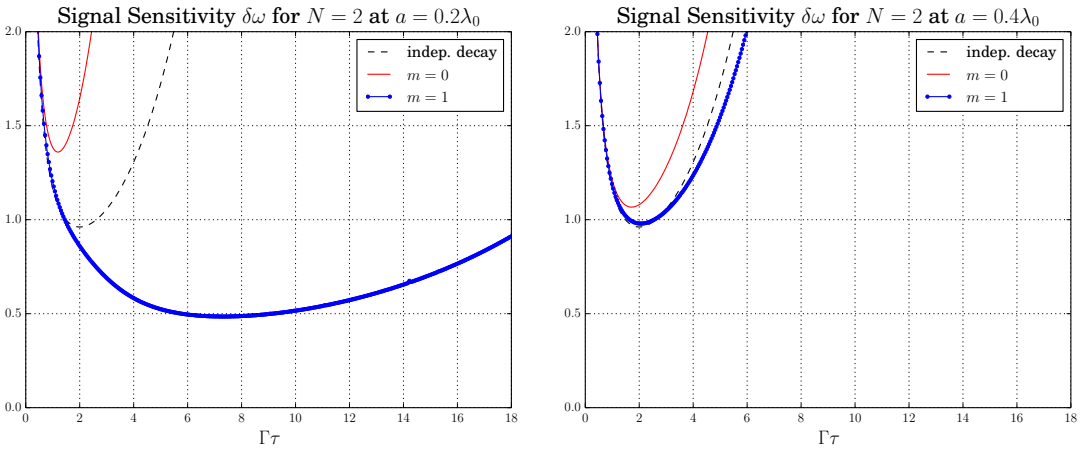

Figure 3.5: *Signal sensitivity of standard and protected Ramsey spectroscopy.* (a) and (b) display the signal sensitivity for two atoms at distances of $a = 0.2\lambda_0$ and $a = 0.4\lambda_0$, respectively. The same distances have been used in (c) and (d). It is clear that for these choices of distances applying the phase rotations enhances the sensitivity. Furthermore, it is clear that smaller distances increase the enhancement achieved by application of phase-spread rotations.

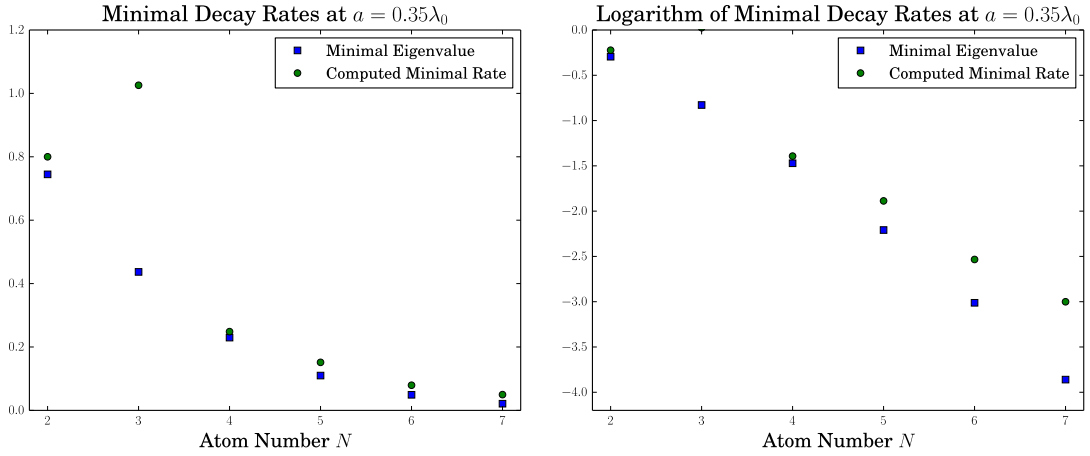

(a) (b)

Figure 3.6: *Scaling of the minimal decay rate.* The scaling of the minimal decay rate as computed in (3.6) with the atom number N is displayed in (a). As a reference the minimal eigenvalue from Fig. 2.3(a) is also shown. The computation has been performed in a chain at distance $a = 0.35\lambda_0$. The larger decay rate for $N = 3$ is due to this particular choice of distance. When considering three atoms at the distance chosen, the negative coupling between the two outermost atoms outweighs the positive nearest-neighbour couplings (see Fig. 2.1 at a distance of $a = 0.7\lambda_0$), effectively reversing the effect of the phase-spread rotations, therefore increasing the decay rate. In (b) the logarithm of the decay rates has been plotted in order to show the exponential scaling of the minimal decay rate with N.

Chapter 4

Protection of a Spin-Squeezed State

For some time now, spin squeezing has been subject to various investigations and applications [16] . The usefulness of spin-squeezed states is therefore obvious, which is owed to the fact that systems that are in a spin-squeezed state have been shown to contain two particle quantum correlations, i.e. entanglement, which is a well-known and useful resource for quantum information.
It is therefore of interest to investigate the lifetime of such spin-squeezed states and whether or not one is able to prolong this lifetime by state protection as it was used in chap. 3.

4.1 Theory of Spin Squeezing

Since spin squeezing itself is not affiliated with the collective effects that cause decay and the reduction of those as is discussed throughout this thesis, a brief theoretical overview will be provided at this point.
An ensemble of N two-level atoms can be treated as an ensemble of pseudo-spin-1/2 particles. Hence, the state of the system can be described by the eigenstates $|S, M\rangle$ of the collective operators S^2 and S_z, as defined in (2.8), where $0 \leq S \leq \frac{N}{2}$ and $|M| \leq S$. Such a state gives rise to a normalized Bloch vector of

$$\boldsymbol{n} = \frac{\langle \boldsymbol{S} \rangle}{|\langle \boldsymbol{S} \rangle|}, \tag{4.1}$$

where $\boldsymbol{S} = (S_x, S_y, S_z)$.

Measure of Squeezing - Squeezing Parameter

Just as it is the case for coherent and squeezed Fock states [17], coherent and squeezed spin states are of minimal uncertainty in the phase space. In terms of operators, these uncertainties of a spin state are given by the variances of operators belonging to a Bloch vector orthogonal to the Bloch vector $\boldsymbol{n}$ itself. Namely, the phase space of a spin

state is the plane perpendicular to the Bloch vector of the state. It is spanned by two perpendicular vectors $\boldsymbol{n}_\perp$ and $\boldsymbol{n}_{\perp'}$ (See Fig. 4.1). One can use these vectors to define

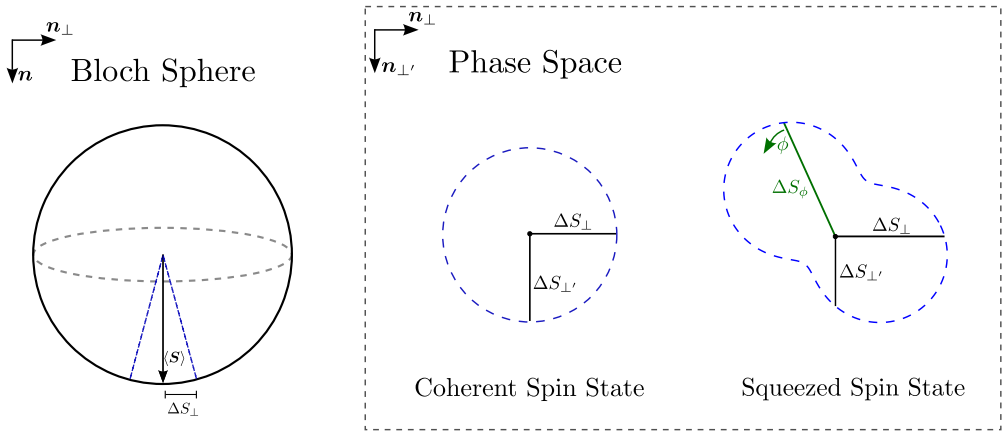

Figure 4.1: *Schematic of phase space of a coherent and squeezed spin state.* As opposed to what one would expect from squeezed Fock states, the phase diagram of a spin-squeezed state does not show an ellipse.

two operators

$$S_\perp = \boldsymbol{n}_\perp \cdot \boldsymbol{S},$$
$$S_{\perp'} = \boldsymbol{n}_{\perp'} \cdot \boldsymbol{S}, \tag{4.2}$$
$$\text{with} \quad \boldsymbol{n} \perp \boldsymbol{n}_\perp \perp \boldsymbol{n}_{\perp'}. \tag{4.3}$$

These operators are conjugate and hence subject to the Heisenberg uncertainty relation,

$$\Delta S_\perp \Delta S_{\perp'} \geq \frac{1}{2} |\langle [S_\perp, S_{\perp'}] \rangle|. \tag{4.4}$$

Here, $\Delta S_\perp = \sqrt{\langle S_\perp^2 \rangle - \langle S_\perp \rangle^2}$ is the variance of the operator $S_\perp$. Using the definition in (4.3) and the commutator relation of the collective operators $[S_i, S_j] = i \sum_k \epsilon_{ijk} S_k$, this relation simplifies to

$$\Delta S_\perp \Delta S_{\perp'} \geq \frac{1}{2} |\langle \boldsymbol{S} \rangle|. \tag{4.5}$$

As it was mentioned, both coherent and spin-squeezed states are of minimal uncertainty, i.e. the uncertainty relation in (4.5) reaches equality for the variances of the respective perpendicular operators. For a coherent spin state, however, both variances are also equal, describing a circle in the phase space while for a spin-squeezed state one is smaller than the other, though they still hold equality in the Heisenberg uncertainty relation as schematically shown in Fig. 4.1.
In order to measure the squeezing of a state, one can define a so-called *Squeezing*

Parameter which shall be denoted as ξ from here on out. There have been many different definitions of such parameters. It will be defined here in such a way that $\xi = 1$ for a coherent spin state and $0 < \xi < 1$ for a squeezed spin state,

$$\xi := \min_{\phi} \left[\frac{\sqrt{N}\Delta S_{\phi}}{|\langle \boldsymbol{S} \rangle|} \right]. \tag{4.6}$$

At this point the variance of the rotated operator S_{ϕ} was used. It is clear that in order for ξ to be a reliable measure of squeezing one has to extremize the variance in the phase space. Hence, one has to rotate one of the perpendicular operators around the Bloch vector of the state and minimize the corresponding variance with respect to the rotational angle ϕ. A rotation of this form can be performed as it was discussed in (2.47), using the Bloch vector as rotational axis and gives rise to the following definition of S_{ϕ},

$$S_{\phi} = e^{i\phi(\boldsymbol{n}\cdot\boldsymbol{S})} S_{\perp} e^{-i\phi(\boldsymbol{n}\cdot\boldsymbol{S})} = S_{\perp} \cos\phi + S_{\perp'} \sin\phi. \tag{4.7}$$

Note, that due to the very definition of the perpendicular operators $S_{\perp}$ and $S_{\perp'}$ their expectation values vanish, which is obvious considering

$$\langle S_{\perp} \rangle = \langle \boldsymbol{n}_{\perp} \cdot \boldsymbol{S} \rangle = \boldsymbol{n}_{\perp} \cdot \langle \boldsymbol{S} \rangle = 0. \tag{4.8}$$

Therefore, the definition of the squeezing parameter further simplifies to

$$\xi = \min_{\phi} \left[\frac{\sqrt{N\langle S_{\phi}^2 \rangle}}{|\langle \boldsymbol{S} \rangle|} \right], \tag{4.9}$$

where the minimization is, as mentioned, performed with respect to the rotational angle ϕ.

Squeezing a Coherent Spin State - One-Axis Twisting

Now that a measure for the amount of squeezing a state contains has been defined, it is of interest how to actually *squeeze* a state. Since the focus here is the protection of such a squeezed state against decay and not on the process of squeezing itself, it is sufficient to make use of the simplest known way to squeeze a state. This is achieved by time evolution of a system with the so-called *One-Axis Twisting Hamiltonian* [16]

$$H_{\chi} = \chi S_{\nu}^2. \tag{4.10}$$

Here, $\nu \in \{x, y, z\}$ has to be chosen according to the state one seeks to squeeze. Squeezing with a poorly chosen operator could leave the state invariant. Note, that to be certain one could also use $S_{\perp}$ as defined in (4.3) instead of S_{ν}. The parameter χ

defines the strength of the squeezing. The Hamiltonian in (4.10) gives rise to a unitary time evolution operator of the form

$$U_\chi(\tau) = e^{-i\chi\tau S_\nu^2}. \tag{4.11}$$

Applying this to a coherent spin state for a certain time τ will yield a squeezed spin state with phase space variances shaped like the one displayed in Fig. 4.1. Note that the time and strength of the squeezing operation have to be small enough for the norm of the Bloch vector to remain sufficiently large. Otherwise the definition of the squeezing parameter given in (4.9) is no longer valid, i.e. $\xi \to \infty$ for $|\langle \boldsymbol{S} \rangle| \to 0$. In general it is sufficient to restrict time and strength to $\chi\tau \ll \pi/4$.

Ground State Squeezing of Two Atoms

At this point a brief example of squeezing a coherent spin state shall be given. It is easy to check that the ground state $|G\rangle = |-\frac{N}{2}, -\frac{N}{2}\rangle$ is a coherent spin state. The normalized Bloch vector simply points in the z-direction and hence the perpendicular operators are S_x and S_y, with respective variances $\Delta S_x = \sqrt{\langle S_x^2 \rangle} = \frac{\sqrt{N}}{2}$ and $\Delta S_y = \Delta S_x$. Therefore, equality in (4.5) is achieved,

$$\Delta S_x \Delta S_y = \frac{N}{4} = \frac{1}{2}|\langle S_z \rangle| = \frac{1}{2}|\langle \boldsymbol{S} \rangle|. \tag{4.12}$$

This means that the ground state is indeed a coherent spin state. One can then arbitrarily choose between S_x^2 and S_y^2 to perform the squeezing operation as defined in (4.11). In the case of two atoms ($N = 2$), the resulting squeezed state $|SS\rangle$ is a superposition of the ground and fully inverted state $|E\rangle$ (neglecting a global phase),

$$|SS\rangle = U_\chi(\tau)\,|G\rangle = \cos\mu\,|G\rangle + i\sin\mu\,|E\rangle\,, \tag{4.13}$$

$$\text{where} \quad \mu := \frac{\chi\tau}{2}. \tag{4.14}$$

As one can see, the state $|SS\rangle$ is basically the GHZ-state $|GHZ\rangle = \frac{1}{\sqrt{2}}(|G\rangle + |E\rangle)$ for $\mu = \frac{\pi}{4}$, which yields a zero-norm Bloch vector and therefore a divergent squeezing parameter. This shows the necessity of the restriction to $\chi\tau \ll \frac{\pi}{4}$.
The variance of the rotated operator S_ϕ as defined in (4.7) is

$$\langle S_\phi^2 \rangle = \cos^2\phi \langle S_x^2 \rangle + \sin^2\phi \langle S_y^2 \rangle + 2\cos\phi\sin\phi \mathrm{Re}\{\langle S_x S_y \rangle\}. \tag{4.15}$$

It is easy to see that $\langle S_x^2 \rangle = \langle S_y^2 \rangle = \frac{1}{2}$ for the squeezed state $|SS\rangle$. Also, it is quite simple to check that $\mathrm{Re}\{\langle S_x S_y \rangle\} = -\cos\mu\sin\mu$. Hence, the variance has a minimum of

$$\min[\langle S_\phi^2 \rangle] = \frac{1}{2} + \min[-2\cos\mu\sin\mu\cos\phi\sin\phi] = \frac{1}{2} - \cos\mu\sin\mu. \tag{4.16}$$

Note that, when plotting $\langle S_\phi^2 \rangle$ as a function of the rotational angle ϕ in a polar plot, the result is a shape similar to the one all the way on the right in Fig. 4.1.
The norm of the Bloch vector is the absolute value of the expectation value $\langle S_z \rangle = -\cos^2 \mu \sin^2 \mu$. Combining all these results, we gain the following expression for the squeezing parameter,

$$\xi = \frac{\sqrt{1 - 2\cos\mu \sin\mu}}{|\cos^2 \mu - \sin^2 \mu|}. \tag{4.17}$$

It is again clear that $\xi < 1$ for $\mu > 0$, as long as one keeps to the restriction that was given before, i.e. $\mu \ll \frac{\pi}{4}$, since ξ will yield an indeterminate division at this point $(\frac{0}{0})$.

4.2 Protection of Spin Squeezing

The basic idea now is to utilize phase-spread rotations like the ones in (2.48) in order to protect such a spin-squeezed state from decay. It will be seen later that such kind of a protection does work indeed. However, it does best for states that have a Bloch vector aligned with the z-axis. This can be explained by the fact that the phase-spread rotations around the z-axis most efficiently protect anything that lies in the xy-plane. The norm of the Bloch vector of a squeezed state, in general, is smaller than the norm of the initial state before the squeezing is performed. Upon decay, the norm of the Bloch vector increases until the vector reaches its full length of $N/2$. Due to the definition of the squeezing parameter ($\xi \propto 1/|\langle \boldsymbol{S} \rangle|$) it is clear that it is larger if the norm is protected more efficiently. Hence, protection of the squeezing parameter of a state that is almost an element of the xy-plane is not favourable.
Note, that the statement that protection is most efficient if the protective rotations are applied about an axis closely aligned to the Bloch vector may motivate the idea of using phase-spread rotations around the Bloch vector itself if the state is far from aligned with the z-axis. Since the Bloch vector changes in time this would require the use of time-dependent phase-spread rotations. However, application of the rotations changes the time evolution of the Bloch vector. Hence, one would need to know the effect of the rotations in order to compute them, making an exact computation of that time evolution impossible. One might be able to make some analytical approximations in order to gain results (see chap. 6), but this goes beyond the purpose of the investigations at this point.

4.3 Results

Due to the complicated dynamics of the treated system analytical methods are quite limited. One can only treat systems of low particle numbers, and even then the analysis is somewhat cumbersome. However, it is possible to simulate the time evolution of larger

systems numerically and investigate the effectiveness of the attempted state protection as discussed before.

4.3.1 Ground State Squeezing of Two Atoms

For purposes of illustrating the principle that is proposed here, it is useful to once again investigate one of the simplest cases of spin squeezing, the squeezing of the ground state of two atoms. It is still possible, even though tedious, to compute the full time evolution of the system and hence the time evolution of the squeezing parameter as well as the effect of the protective phase-spread rotations as they have been proposed. The squeezed ground state of two atoms $|SS\rangle$ as it was computed in (4.13) gives rise to a density matrix of the form

$$\rho_0 = \cos^2\mu\,|G\rangle\langle G| + \sin^2\mu\,|E\rangle\langle E| + i\cos\mu\sin\mu(|E\rangle\langle G| - |G\rangle\langle E|). \tag{4.18}$$

It is easy to see that this state has a normalized Bloch vector of $\boldsymbol{n} = (0, 0, -1)$. For a time-dependent density matrix, the expectation values of S_x and S_y are

$$\begin{aligned}\langle S_x\rangle &= \mathrm{tr}(S_x\rho(t)) = \sqrt{2}\mathrm{Re}\{\rho^{ES}(t) + \rho^{SG}(t)\},\\ \langle S_y\rangle &= -\sqrt{2}\mathrm{Im}\{\rho^{ES}(t) + \rho^{SG}(t)\}.\end{aligned} \tag{4.19}$$

Making use of the master equation as it was defined in (2.13), one can write the differential equations for the density matrix elements $\rho^{ES}(t)$ and $\rho^{SG}(t)$, respectively,

$$\dot{\rho}^{ES} = -\frac{1}{2}(\gamma_S + 2\Gamma - 2i(\Delta - \Omega))\rho^{ES}, \tag{4.20}$$

$$\dot{\rho}^{SG} = -\frac{1}{2}(\gamma_S - 2i(\Delta + \Omega))\rho^{SG} + \gamma_S\rho^{ES}. \tag{4.21}$$

At this point the following definitions were used.

$$\begin{aligned}&\Gamma_{12} = \gamma, \quad \Gamma_{11} = \Gamma_{22} = \Gamma, \quad \Omega_{12} = \Omega,\\ &\gamma_S = \Gamma + \gamma, \quad \gamma_A = \Gamma - \gamma.\end{aligned} \tag{4.22}$$

Since the equation in (4.20) is homogeneous, it is clear that $\rho^{ES}(t) \propto \rho^{ES}(0)$ and, since $\rho^{ES}(0) = 0$ for the initial state under consideration, it follows that $\rho^{ES}(t) = 0\ \forall\ t$. This fact also makes the differential equation for ρ^{SG} homogeneous and one can simply follow the same argumentation as before, to the end that $\langle S_x\rangle = \langle S_y\rangle = 0\ \forall\ t$. Therefore, the Bloch vector of the state points in z-direction and its norm is $|\langle \boldsymbol{S}\rangle| = |\langle S_z\rangle|\ \forall\ t$.
One therefore only needs to compute $\langle S_z\rangle$ and $\langle S_\phi^2\rangle$ in order to find the time evolution of the squeezing parameter,

$$\langle S_z\rangle = \rho^{EE}(t) - \rho^{GG}(t) = 2\rho^{EE} + \rho^{SS} + \rho^{AA} - 1, \tag{4.23}$$

$$\langle S_\phi^2\rangle = \mathrm{Re}\{e^{-2i\phi}\rho^{GE}(t)\} + \frac{\rho^{SS}(t) - \rho^{AA}(t)}{2} + \frac{1}{2}. \tag{4.24}$$

The phase-spread rotations that are to be used for two atoms, take the simple form

$$R_z = \prod_j e^{i\pi(j-1)\sigma_z^{(j)}/2} = e^{i\frac{\pi}{2}\sigma_z^{(2)}}, \tag{4.25}$$

and as it was mentioned before have the effect of interchanging the occupation of the symmetric state $|S\rangle$ and the asymmetric state $|A\rangle$ and vice versa. The other states ($|G\rangle$ and $|E\rangle$) remain invariant under rotations around the z-axis. Hence, the sole effect of the phase-spread rotations is to swap the populations ρ^{SS} and ρ^{AA}. For simplicity, it therefore makes sense to define a function that contains these populations, so one has to consider the effect on this function only rather than on the entire expectation values,

$$g^{\pm}(t) := \rho^{SS}(t) \pm \rho^{AA}(t), \tag{4.26}$$

$$R_z g^{\pm}(t) = \pm g^{\pm}(t). \tag{4.27}$$

It is obvious that $0 \leq g^{+}(t) \leq 2 \; \forall \; t$. Since the decay rate γ_S of the symmetric state is larger, the population of the symmetric state is also larger in the beginning, and therefore it holds that $0 \leq g^{-}(t) \leq 1$ for sufficiently small times. However, since at some point all population except for the asymmetric state will have decayed to the ground state, $g^{-}(t)$ can actually be negative at large times.
Note, that from the invariance of the states $|E\rangle$ and $|G\rangle$ under rotations about the z-axis follows that the initial squeezed state $|SS\rangle$ is only changed by a local phase upon application of the phase-spread rotation. This local phase, though, is irrelevant in the time evolution of the squeezing parameter, rendering the first protective rotation useless. It will, however, be seen that the second rotation applied after some time will enhance the squeezing that has not decayed up to that time.
Again, using the master equation, one can write the differential equations for all necessary density matrix elements,

$$\dot{\rho}^{EE} = -2\Gamma\rho^{EE}, \tag{4.28}$$

$$\dot{\rho}^{SS} = \gamma_S(\rho^{EE} - \rho^{SS}), \tag{4.29}$$

$$\dot{\rho}^{AA} = \gamma_A(\rho^{EE} - \rho^{AA}), \tag{4.30}$$

$$\dot{\rho}^{GE} = -(\Gamma + 2i\Delta)\rho^{GE}. \tag{4.31}$$

These differential equations can readily be solved as

$$\rho^{EE}(t) = \sin^2\mu e^{-2\Gamma t}, \tag{4.32}$$

$$g^{\pm}(t) = \frac{\sin^2\mu}{\gamma_S\gamma_A}\left(\gamma_S^2(e^{-\gamma_S t} - e^{-2\Gamma t}) \pm \gamma_A^2(e^{-\gamma_A t} - e^{-2\Gamma t})\right), \tag{4.33}$$

$$\mathrm{Re}\{e^{-2i\phi}\rho^{GE}(t)\} = e^{-\Gamma t}\cos\mu\sin\mu\sin 2(\phi - \Delta t). \tag{4.34}$$

The expectation values (4.23) and (4.24) are then

$$\langle S_z\rangle = 2\sin^2\mu e^{-2\Gamma t} + g^{+}(t) - 1, \tag{4.35}$$

$$\langle S_\phi^2\rangle = \frac{1}{2}\left(1 + g^{-}(t)\right) - e^{-\Gamma t}\cos\mu\sin\mu\sin 2\phi, \tag{4.36}$$

where resonance ($\Delta = 0$) was assumed. The squeezing parameter is proportional to the variance of the rotated operator (4.36), and hence minimization over the angle ϕ gives $\min_\phi[-\sin 2\phi] = -1 \; \forall \; t$. Combining all these results, we obtain a time-dependent

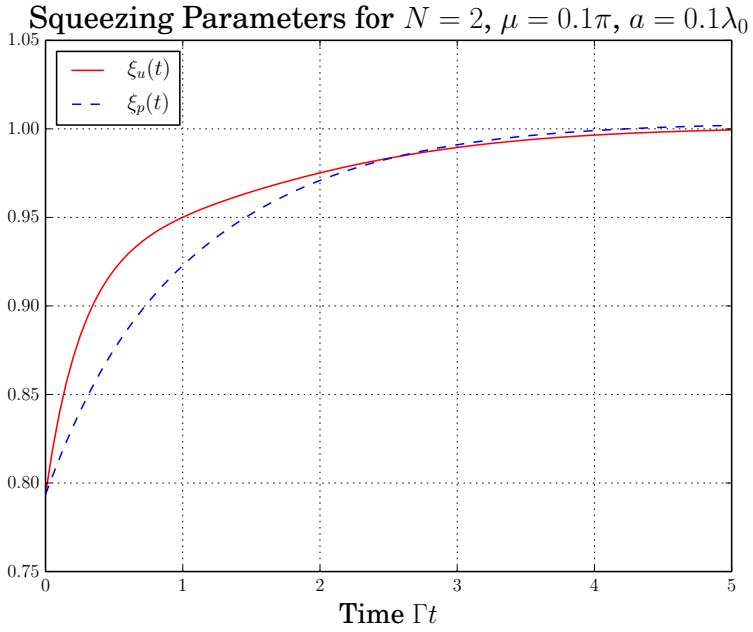

Figure 4.2: *Squeezing parameters for squeezing of the two atom ground state.* The distance between the two atoms was chosen to be $a = 0.1\lambda_0$, with an initial squeezing strength of $\mu = 0.1\pi$. Clearly, the squeezing parameter where the phase-spread rotation was applied, $\xi_p(t)$, is smaller at shorter times than the freely decaying squeezing parameter $\xi_u(t)$.

squeezing parameter of the form

$$\xi_u(t) = \frac{\sqrt{1 + g^-(t) - 2e^{-\Gamma t}\cos\mu\sin\mu}}{|2\sin^2\mu e^{-2\Gamma t} + g^+(t) - 1|}. \tag{4.37}$$

Note, that since $g^\pm(0) = 0$, it is easy to see that $\xi_u(0)$ is identical to the squeezing parameter gained for the initial state in (4.17). This expression for the time-dependent squeezing parameter does not include any manipulation by the phase-spread rotations and can therefore be considered the time evolution of *unprotected* squeezing.
The original idea of protecting the squeezing against decay was to apply phase-spread rotations to the initial state and then undo them after a time evolution. However, as it was mentioned, the decay of the squeezing in the initial state is not affected by rotations around the z-axis. The only effect of protection one can hope to achieve is hence at the point when the phase-spread rotations are undone. It is easy to see that the effect of R_z^{-1} is the same as for R_z, as shown in (4.27). So, when R_z^{-1} is applied after some

time, $g^+(t)$ remains invariant and so does $|\langle S_z \rangle|$, as it would be expected for a rotation around the z-axis. On the other hand, $g^-(t)$ changes sign and the squeezing parameter for the *protected* case ξ_p is thus

$$\xi_p(t) = \frac{\sqrt{1 - g^-(t) - 2e^{-\Gamma t} \cos \mu \sin \mu}}{|2 \sin^2 \mu e^{-2\Gamma t} + g^+(t) - 1|}. \tag{4.38}$$

Since for sufficiently small times $0 \leq g^-(t) \leq 1$, it is obvious that $\xi_p(t) \leq \xi_u(t)$ at those times, meaning that the protected state is more squeezed than when there are no protective rotations. For larger times $g^-(t)$ can be negative, though, and hence the phase-spread rotation destroys some squeezing rather than enhancing it. The squeezing parameters are plotted in Fig. 4.2, where all the discussed points can be seen graphically. In this specific case, since the first protective phase-spread rotations do not have any effect on the initial state, 'state protection' is a poor choice of terminology. It would actually be more precise to call the procedure 'squeezing enhancement', since it simply enhances the squeezing that is left in the state. For quite large times the squeezing is destroyed rather than enhanced until the squeezing has fully decayed and the state is once again invariant under rotation around z-axis. This is the case when the state has decayed to the ground state. Note, that the mentioned invariance of the initial state is restricted to this very special case of squeezing a two-atom state that has a Bloch vector aligned with the z-axis. If it was a state that had a Bloch vector that has some expansion in another direction or simply just a larger number of atoms under consideration, this would no longer be the case and the term 'state protection' would once more become accurate. However, analytical discussion of the time evolution of such states is somewhat more involved and goes beyond the purpose of illustrating the efficiency of our procedure.

4.3.2 Numerical Results for Larger Systems

Now that the principle workings of the protected scheme have been discussed and shown for two atoms, one can extend the results to larger systems using numerical methods. However, due to the high dimension of the Hilbert space (2^N), one is again limited to atom numbers that are sufficiently small ($N < 10$). In this region, though, it can be shown that the protective scheme works quite well and, once again, protection is even more efficient for larger numbers of atoms due to the reduced minimal decay rate.

Ground State Squeezing

First off, one can again consider the simplest case of squeezing the ground state, but for a larger number of atoms. Furthermore, it can be shown that the optimal m for the phases $\varphi_j^{(m)}$ is once again $m = N/2$, i.e. the integer restriction of m breaks down for odd atom numbers, in order to allow for a phase shift of π between nearest neighbour

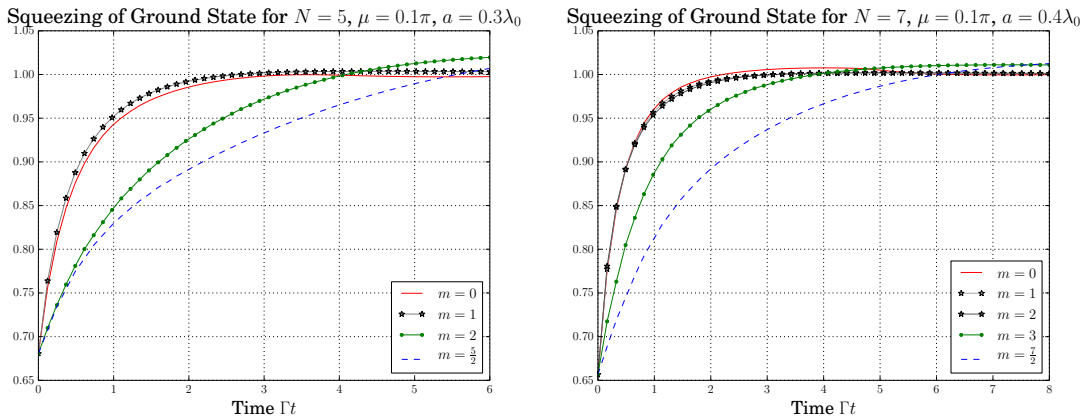

(a) (b)

Figure 4.3: *Squeezing parameters for odd numbers of atoms.* (a) shows the squeezing parameters for ground state squeezing of $N = 5$ atoms at distance $a = 0.3\lambda_0$ with different phase-spread rotations applied $m = 0, ..., N/2$. (b) shows the same setup but for $N = 7$ atoms at distance $a = 0.4\lambda_0$. From both plots it is clear that, for an odd number of atoms N the optimal m is no longer an integer, but a half integer, namely $m = N/2$.

atoms, as can be seen in Fig. 4.3. From here on out only two cases shall be considered: the unprotected squeezing parameter $\xi_u(t)$ shall correspond to $m = 0$ and the protected squeezing parameter $\xi_p(t)$ to $m = N/2$, respectively.
It was previously mentioned that protection of squeezing works best for states that have Bloch vectors aligned with the z-axis. To this end it is of course necessary to compare the results. In Fig. 4.3 it can already be seen that this protection of squeezing works quite well for the ground state of a chain of N atoms. Note, that compared to the other applications in this thesis that focus on reduction of decay, larger distances of the atoms in the chain have been chosen. This is due to the fact that for extremely small distances the dipole-dipole interaction becomes strong enough to cause oscillatory behaviour in the squeezing parameter due to its coherent redistribution of population. Also, the decay of the protected squeezing parameter $\xi_p(t)$ would take much longer due to the further reduced decay rate which would in turn make the computation of longer time evolutions necessary. Hence, to keep matters numerically simple and since it is sufficient to demonstrate the principle, larger distances have been chosen.

Squeezing Arbitrary States

Now that the efficiency for the procedure of protection for an initial state with a Bloch vector aligned with the z-axis was shown, it is of interest to investigate states that are not of that form. To this end it shall be sufficient to consider states that have been rotated around the y-axis by an angle α from the ground state and therefore have a

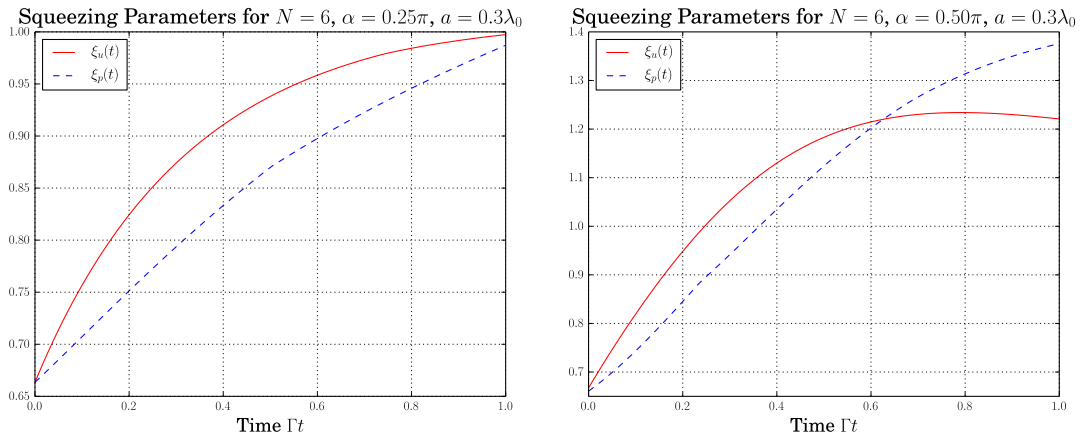

(a) (b)

Figure 4.4: *Squeezing of states with higher excitation.* Both plots present the squeezing parameter $N = 6$ atoms at a distance of $a = 0.3\lambda_0$. (a) shows the vastly faster decay of the state that is rotated around the y-axis by $\alpha = \pi/4$ compared to the case of ground state squeezing ($\alpha = 0$), while (b) shows the even faster decay for a rotation by $\alpha = \pi/2$.

Bloch vector with some expansion in the x-direction. To particularize, these states are of the form

$$|\psi_\alpha\rangle = R_y[\alpha]\,|G\rangle = e^{i\alpha S_y}\,|G\rangle\,. \tag{4.39}$$

The closer α is to π, the larger the number of excitations in the state $|\psi_\alpha\rangle$ and hence its decay rate. It is possible, however, to protect the squeezing against decay up to some point. The decay is so fast that even though making use of the protective rotations is useful, the squeezing still decays quite fast. This is illustrated in Fig. 4.4.

Chapter 5

Preparation of a Robust Multipartite State

Investigation of methods as to how to reduce or even minimize the decay of a chain of two-level atoms has been the focus up to this point. Now, however, one seeks to eliminate the need for such methods by restricting all excitations of the system to the state that has the lowest decay rate, i.e. the longest lifetime. It will be shown that it is possible to coherently drive the system such that eventually close to all population ends up in this state of lowest decay rate. This driving is achieved by resonant addressing of the state (energy conservation). However, there is still a need for the phases (2.28) that have been used in every application so far. These phases have to be imprinted on the system by a laser used to perform the excitation. The experimental realization of such a phase imprinting may pose some technical difficulties as one needs control over the system on the level of individual two-level emitters, which will also be addressed in this chapter.

5.1 Driving Scheme

Using a laser in order to coherently drive a system can mathematically be described by a Hamiltonian of the form

$$H_\eta(t) = \sum_{j=1}^{N} (\eta_j \sigma_j^+ e^{-i\frac{\omega_l t}{2}} + \eta_j^* \sigma_j^- e^{i\frac{\omega_l t}{2}}). \tag{5.1}$$

Here, ω_l is the frequency of the laser. The strength with which the j-th atom is driven is governed by the parameter η, which is modified by the arbitrary phases $\{\phi_j\}_{j=1}^N$,

$$\eta_j := \eta e^{-i\phi_j}. \tag{5.2}$$

The complete Hamiltonian for the time evolution of the system when driven by $H_\eta(t)$ is then

$$H(t) = H_0 + H_{dip} + H_\eta(t). \tag{5.3}$$

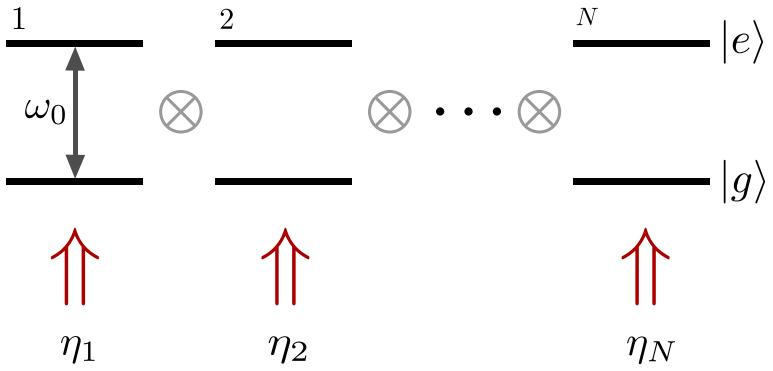

Figure 5.1: *Schematics illustrating the asymmetric driving.* The driving strength η is modified by the phase ϕ_j for the j-th atom in a chain of N atoms. Due to transverse driving no further phases are acquired by the laser.

The time-dependence can be eliminated by a simple transformation into the interaction picture. This is most convenient and hence the investigation of the time evolution will be carried out in this picture, where the complete Hamiltonian is of the form

$$H = \frac{\Delta}{2}\sum_{i=1}^{N}\sigma_z^{(i)} + \sum_{i\neq j}\Omega_{ij}\sigma_i^+\sigma_j^- + \sum_{j=1}^{N}(\eta_j\sigma_j^+ + \eta_j^*\sigma_j^-), \tag{5.4}$$

where $\Delta = \omega_0 - \omega_l$ is the detuning between the atomic transition and the laser frequency. All examples given so far show that reducing the decay in a system requires a reduction of symmetry of the state the system is in. Hence, one can anticipate that the state of lowest possible decay rate is one of minimal symmetry. When driving the system with a Hamiltonian without phases, i.e. $\phi_j = 0\,\forall\, j$ $(\eta_j = \eta)$, one can only excite the symmetric states. This is where the form of the phases as they have been introduced above becomes of importance. At this point no further definition of the phases $\{\phi_j\}_{j=1}^N$ will be given, but it shall be mentioned that just as it was for the phase states in the single-excitation manifold (2.27), a phase shift of π between nearest neighbours will prove to be most favourable for our purpose. This will also be discussed later on. A general transverse driving with H_η of a chain of atoms is illustrated in Fig. 5.1.

Imprinting phases, however, is not sufficient to drive the state of lowest symmetry. If there are no energy shifts, e.g. by dipole-dipole interaction, states that possess the same number of excitations also have the same energy and are therefore highly degenerate. Since a state of a low decay rate has a very narrow linewidth while a state of large decay rate has a broad one (Lorentzian line shapes), they cannot be energetically separated in a reliable way, even if the degeneracy is lifted. In order to achieve sufficient energy separation the system needs to be subject to quite large energy shifts. Fortunately, such shifts can readily be implemented by taking advantage of the dipole-dipole interaction Ω_{ij}. This interaction causes energy shifts lifting the degeneracy and due to the fact that $\Omega_{ij} \to \infty$ as $a \to 0$ (See Fig. 2.1), one simply has to place the atoms in the chain very

close together ($a \approx 0.1\lambda_0$). This energy shift and lifting of degeneracy is schematically shown in Fig. 5.2(a). The amount by which a state $|\psi\rangle$ gets shifted can be computed by

$$\Delta\omega = \langle\psi| H_{dip} |\psi\rangle . \tag{5.5}$$

It will be shown that the state that possesses the lowest decay rate is subject to the maximally negative dipole shift.

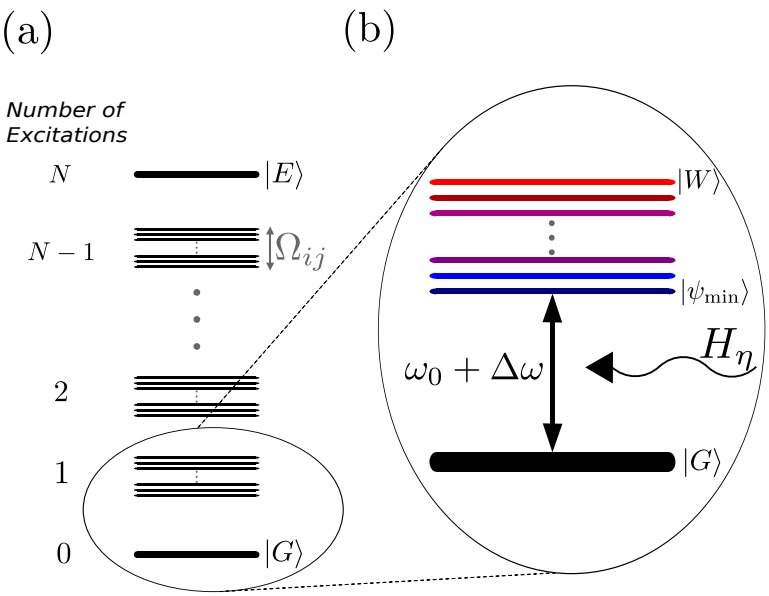

Figure 5.2: *Schematics showing the excitation subspaces with dipole-dipole interaction present.* (a) illustrates the effect of the dipole interaction Ω_{ij} lifting the degeneracy in the excitation subspaces. (b) shows the driving of the transition to the state of lowest decay rate $|\psi_{min}\rangle$ in the single-excitation subspace by H_η. The state is shifted by an amount of $\Delta\omega$ due to the dipole-dipole coupling.

5.2 Energetic Properties of the Longest-Lifetime State

As a first step towards numerical simulation of the dynamics, it is of interest to investigate the properties of the state possessing the minimal decay rate (longest lifetime). This specific state shall be called $|\psi_{min}\rangle$.
In order to find the state with the lowest decay rate one can neglect the coherences between the states and simply investigate the decrease of the population in time. All eigenstates are a superposition of states containing the same amount of excitations (in the bare basis) and the action of the raising and lowering operators $\sigma_j^{\pm}$ on states of that form is known. We can therefore obtain an equation for the decay rate of a state $|\psi\rangle$ as

it was found for the phase states in the single-excitation subspace from (2.38).

$$\gamma_\psi = \sum_{j,k=1}^{N} \Gamma_{jk} \mathrm{Re}\{\langle\psi| \sigma_j^+ \sigma_k^- |\psi\rangle\} = \sum_{j,k} \Gamma_{jk} \mathrm{Re}\{\mathrm{tr}(\sigma_j^+ \sigma_k^- |\psi\rangle \langle\psi|)\} \tag{5.6}$$

Even though the decay rate as computed in (5.6) is not exact (coherent coupling to other states with the same number of excitations was discarded), it is sufficient in order to find the minimum.

Number of Excitations

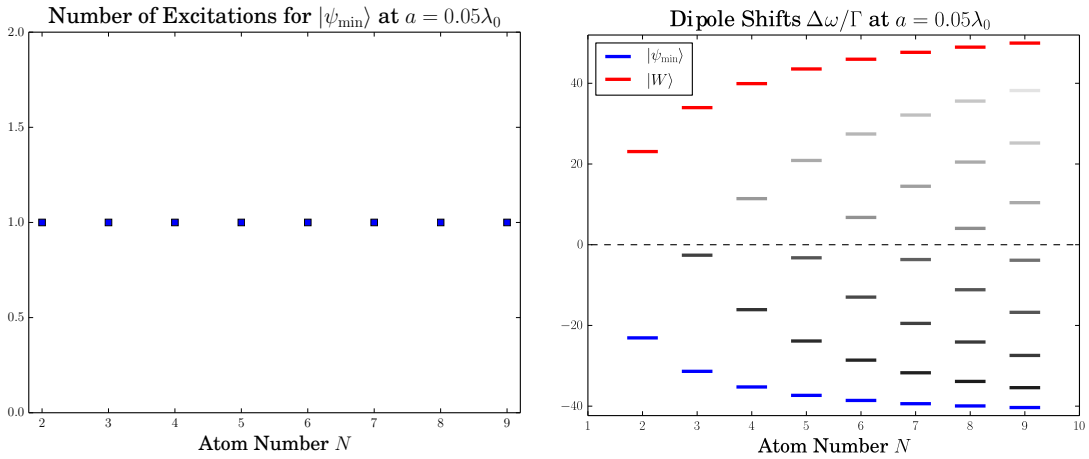

(a) (b)

Figure 5.3: *Number of excitations for state of lowest decay rate and dipole shifts.*(a) shows that the state with the lowest decay rate contains only one excitation, as computed by (5.7). (b) displays the dipole shifts of all states in the single-excitation subspace for different atom numbers. The state with the lowest decay rate $|\psi_{min}\rangle$ is subject to the maximally negative dipole shift, while the super-radiant state of highest symmetry $|W\rangle$ is shifted maximally positively.

One question of interest is how many excitations the state of lowest decay rate actually holds. It was mentioned before that due to the minimal number of couplings this state has to be in the subspace which contains only a single excitation. At this point a numerical investigation of this shall be provided, undermining this claim. The state with the lowest possible decay rate is found by minimizing (5.6). Since all states are eigenstates of the collective operator S_z with eigenvalues that range from $-\frac{N}{2}$ to $\frac{N}{2}$ (in integer steps), the number of excitations n_ψ in a state $|\psi\rangle$ can simply be computed by

$$n_\psi = \langle\psi| S_z |\psi\rangle + \frac{N}{2}. \tag{5.7}$$

In Fig. 5.3(a) it can be seen that up to a sufficiently large number of atoms N the state of lowest decay rate does indeed only contain a single excitation. This may also be true in general, i.e. for any number of atoms in a chain configuration. Since this, however, would require an analytical expression for the decay rate of a state for an arbitrary number of atoms containing an arbitrary amount of excitations, no further proof will be provided.

Dipole Shifts

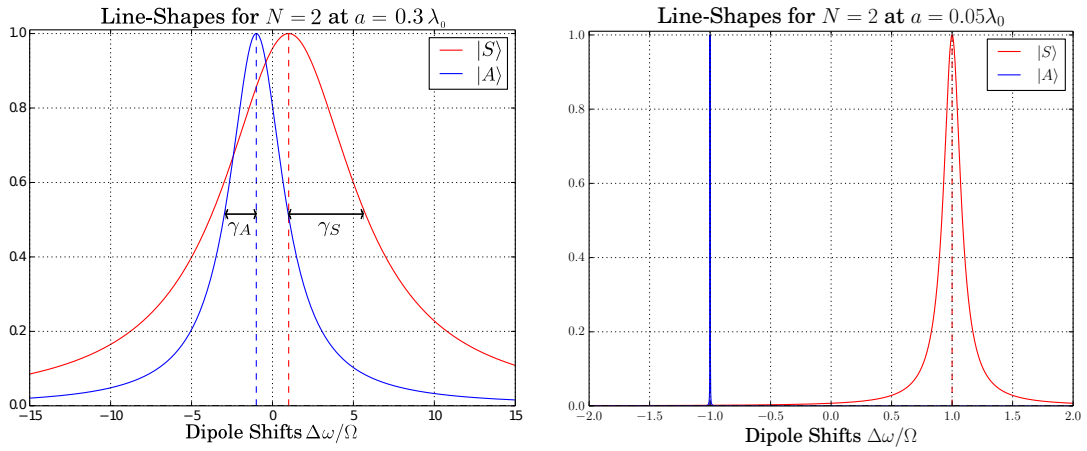

(a) (b)

Figure 5.4: *Lorentzian line shape functions.* The line shapes of the symmetric and asymmetric state in the case of $N = 2$ atoms are illustrated. Their linewidths are given by their respective decay rates $\gamma_S = \Gamma + \gamma$ and $\gamma_A = \Gamma - \gamma$ with $\Gamma_{ii} = \Gamma$ and $\Gamma_{12} = \gamma$. The shifts of the center of the lines have been plotted in units of the dipole-dipole coupling $\Omega_{12} = \Omega_{21} = \Omega$. It is clear that the asymmetric state $|A\rangle$ is shifted by $-\Omega$ while the symmetric state is shifted by $+\Omega$. (a) shows them at a distance of $a = 0.3\lambda_0$, where the states clearly show a significant overlap, as opposed to (b) where the dipole shifts are strong enough to truly separate the lines. This is due to the vastly increased strength of the shifts at the distance $a = 0.05\lambda_0$.

Now that it was established that one only needs to work with states containing a single-excitation, it is of further interest to investigate the dipole shift of the state of minimal decay rate, as computed in (5.5). The shifts of the states in the single-excitation subspace are shown in Fig. 5.3(b). Just as it was the case for the phase states in the single-excitation manifold, the state of lowest decay rate is subject to the maximally negative dipole shift (for comparison see Fig. 2.8). Note, that Fig. 5.3(b) is not a schematic, the dipole shifts for all states have been computed numerically. The fact that one can restrict the computation to the single-excitation subspace already yields a

significant advantage in computational time even though the results in Fig. 5.3(b) did not require a full time evolution of the system.
It has also been mentioned that the dipole shifts have to be large enough in order to energetically separate the spectral lines of the states from one another. This separation of the line shape functions is shown in Fig. 5.4.

5.3 Artificial Phases

The choice of phases for the driving as it is illustrated in Fig. 5.1 is of course of utmost importance for the efficiency of the driving. For a first test of the proposed procedure, one can simply choose the phases $\{\phi_j\}_{j=1}^N$ in (5.2) to be the phases $\{\varphi_j^{(m)}\}_{j=1}^N$ as they have been used before (see (2.28)). Furthermore, one can choose the index m to be optimal, namely $m = N/2$. It shall be stated at this point that, even though m was previously restricted to be an integer, the choice of the phases is now completely arbitrary. Hence, one can also choose m arbitrarily. It has been checked, however, that even for odd numbers of atoms, the choice $m = N/2$ is optimal. This gives phases of

$$\phi_j = \varphi_j^{\left(\frac{N}{2}\right)} = \pi(j-1), \tag{5.8}$$

and therefore a driving Hamiltonian

$$H_\eta = \eta \sum_j \left(\sigma_j^+ e^{-i\pi(j-1)} + \sigma_j^- e^{i\pi(j-1)}\right). \tag{5.9}$$

However, this shall only serve as a test of the procedure, since it is in no way physically justified to choose the phases in such a way. One could argue that, when driving longitudinal, i.e. in the direction of the atom chain, the laser acquires a phase-shift of $e^{ik_l a}$ when travelling from one atom to the next. In order for $k_l a = \pi$, however, the atoms would need to be separated by a distance of $a = 0.5\lambda_0$ (assuming resonance, i.e. $k_l = k_0$). This distance does not result in sufficient energy shifts by dipole-dipole interaction for the states to be energetically well separated and is therefore undesirable. Note also, that only transverse driving is considered here, i.e. the laser does not acquire any phases in between particles due to propagation (See Fig. 5.1).

5.3.1 Two Atom Case

Once again, the simplicity of treating only two atoms proves useful to gain some analytical insight. The complete Hamiltonian, including phases in the driving, for $N = 2$ is

$$H = \frac{\Delta}{2}(\sigma_z^{(1)} + \sigma_z^{(2)}) + \Omega(\sigma_1^+\sigma_2^- + \sigma_2^+\sigma_1^-) + \eta(\sigma_1^+ - \sigma_2^+ + \sigma_1^- - \sigma_2^-). \tag{5.10}$$

Since the system is initially in the ground state, it makes sense to consider the action of the phase-driving operator $(\sigma_1^+ - \sigma_2^+)$. Straight forward application of this operator yields

$$(\sigma_1^+ - \sigma_2^+)\,|G\rangle = \sqrt{2}\,|A\rangle\,. \tag{5.11}$$

The asymmetric state $|A\rangle$ is the state with the longest lifetime (decay rate $\gamma_A = \Gamma - \gamma$). This action of the operator therefore shows that the phase-imprinting is successful when attempting to drive the asymmetric state. However, since

$$(\sigma_1^+ - \sigma_2^+)\,|A\rangle = -\sqrt{2}\,|E\rangle\,, \tag{5.12}$$

one still needs to make use of the dipole shifts in order to tune this transition to the fully inverted state $|E\rangle$ far off-resonant. Otherwise, the system would saturate at a point where half the population is in the asymmetric state and driving into and out of this state is hence of equal probability. Also, as it was mentioned before, the energetic separation of the symmetric and asymmetric state needs to be sufficiently large. Fortunately, this is also achieved with the dipole shifts (See Fig. 5.4).
Given sufficiently large dipole shifts one then needs to match the laser frequency to the transition from the ground to the asymmetric state. Namely, since the dipole shift on the asymmetric state is

$$\Delta\omega_A = \langle A|\,H_{dip}\,|A\rangle = -\Omega, \tag{5.13}$$

the detuning has to be chosen as

$$\Delta = \omega_0 - \omega_l = \omega_0 - (\omega_0 - \Omega) = \Omega. \tag{5.14}$$

Unfortunately, even for the two-atom case analytical investigation is limited. It shall be stated here that the full time evolution was computed numerically and has yielded results very similar to the ones shown for larger numbers of atoms in the following section.

5.3.2 Numerics

The driving with these artificial phases can be extended to a full time evolution even for larger atom chains and yields great results, making a physical realization of the phases as they are in (5.8) highly desirable. Note, that the detuning Δ in the Hamiltonian (5.4) once again has to be matched to the transition frequency to the state of minimal decay rate $|\psi_{min}\rangle$, including the dipole shifts as computed in (5.5). Namely, the frequency of the driving laser has to be $\omega_l = \omega_0 + \Delta\omega_{min}$, and hence

$$\Delta = \omega_0 - \omega_l = -\Delta\omega_{min} = \langle\psi_{min}|\,H_{dip}\,|\psi_{min}\rangle\,. \tag{5.15}$$

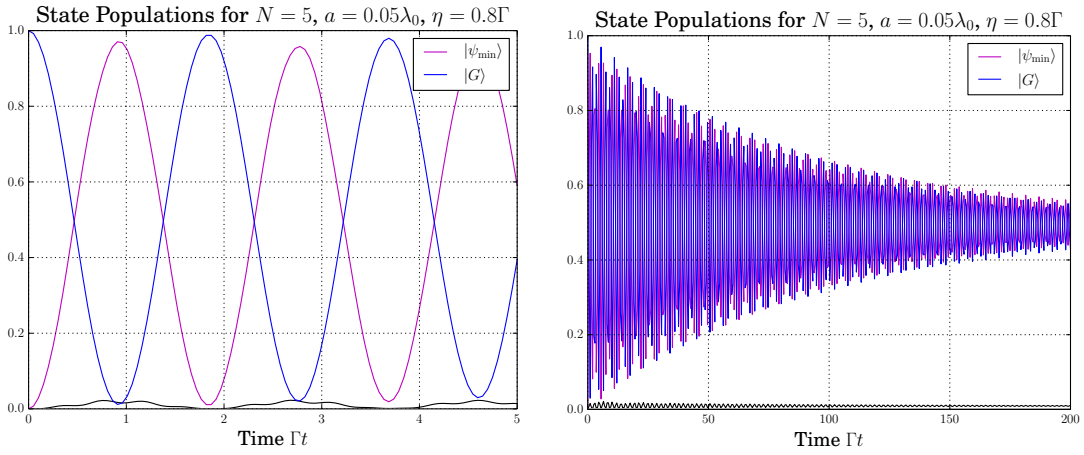

(a) (b)

Figure 5.5: *Driving the state of lowest decay rate with artificial phases.* At a distance of $a = 0.05\lambda_0$ in a five atom chain with a pump strength of $\eta = 0.8\Gamma$, (a) shows that the driving results in almost perfect Rabi oscillations with small (negligible) population in states of higher excitations due to two-photon processes. (b) displays the saturating process of the system when driving for long times. The efficiency displayed justifies the choice for the artificial phases.

In Fig. 5.5 it can be seen just how efficient the procedure is when working with artificial phases since the system displays almost perfect Rabi oscillations between the ground state and the state of lowest decay rate. Larger numbers of particles make the procedure more difficult due to more long-range, i.e. positive dipole-dipole couplings. It is therefore harder to energetically separate states for a chain of many atoms, hence when driving one will populate states of larger decay rate in the system.
Also, as it is expected for a driving of a two level transition, given large enough times the system will acquire a steady state, i.e. saturate at a point where both the ground state and the state of minimal decay rate possess a population of 1/2 (See Fig. 5.5(b)). It has now been established that the procedure works in a somewhat efficient way. Instead of driving the system in a saturated state, however, one might aim to perform a π-pulse and then let the state decay freely, namely defining the pump strength as a function of time, such that

$$\eta(t) = \eta_0(\theta(\tau - t) - \theta(t)) \tag{5.16}$$

where $\theta(t)$ is the Heaviside function. This is illustrated in Fig. 5.6(a) and Fig. 5.6(b) shows just how slow the state decays. The simulations so far have been done on a complete, realistic system driven with artificial phases. In order to extend to larger atom numbers, one can again use the fact that the state of interest lies in the single-excitation subspace. This will, however, neglect any two-photon processes that would lift the

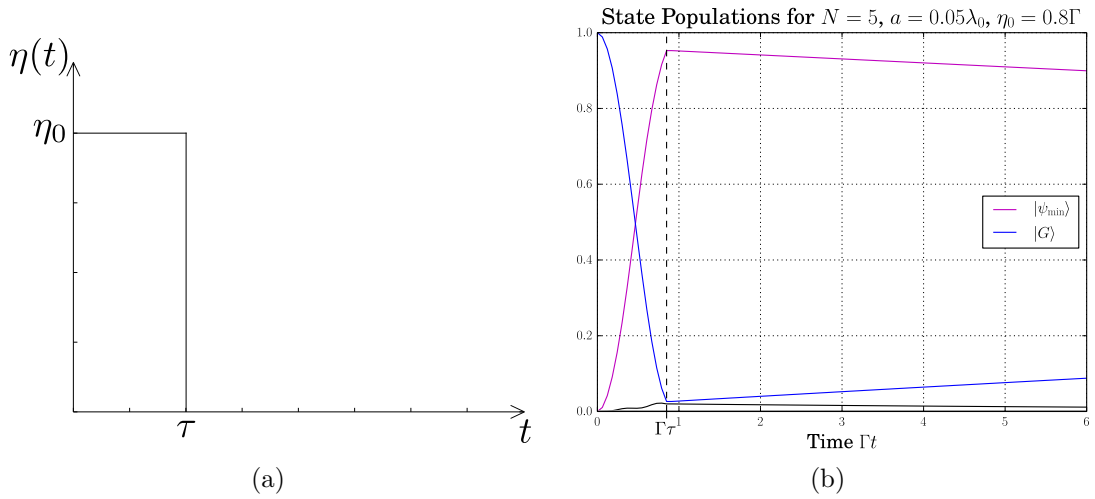

(a) (b)

Figure 5.6: *π-pulse scheme.* (a) schematically shows $\eta(t)$ as it is defined in (5.16). (b) shows the numerical result when applying a pumping of that form, yielding an almost perfect π-pulse from $t = 0$ to $t = \tau$, followed by the extremely slow free decay of the populated state.

system into states of higher excitations and hence is only valid for extremely small distances between the atoms in the chain ($a \approx 10^{-2}\lambda_0$). Still, this is an approximation, but it is sufficient to show that the proposed procedure works even for large numbers of atoms. Results for more particles that can be computed easily due to the simplified numerics are shown in Fig. 5.7 and essentially yield the same results as before.

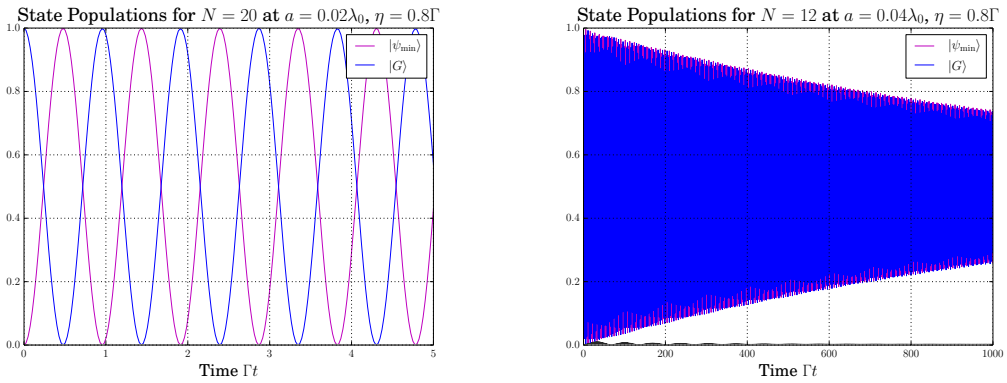

(a) (b)

Figure 5.7: *Driving with artificial phases in the single-excitation subspace.* (a) The efficiency of the procedure for large numbers of particles, i.e. $N = 20$, can be shown due to the reduced numerical effort. (b) shows how much slower the system saturates due to the vastly lower decay rate in the case of larger atom numbers, $N = 12$.

5.4 Utilizing a Magnetic Field Gradient

The discussion up to this point has revolved around driving a system with phases in the driving Hamiltonian. The question that has yet to be answered, however, is how to realistically construct a driving of such a form. It was established that the procedure works quite efficiently for a phase shift of π between nearest neighbour atoms in a chain. In order to realize this, one can make use of a magnetic field gradient. A magnetic field will simply introduce an energy shift of the atom levels via the Zeeman effect that is linear in the strength of the field B. It is therefore valid to scale the detuning with the atom index, providing a modified Hamiltonian of the form

$$H_0^B = \frac{\Delta}{2}\sum_{i=1}^{N}\sigma_z^{(i)} + \Delta_B\sum_{i=1}^{N}(i-1)\sigma_i^+\sigma_i^-, \tag{5.17}$$

where $\Delta_B(i-1)$ is the energy shift of the excited state of the i-th atom in the chain. The magnetic field is set to be zero at the position of the first atom, hence this atom does not experience any energy shift by the field. This is displayed schematically in Fig. 5.8. The system shall then be driven by a pumping Hamiltonian without phases ($\phi_j = 0\ \forall\ j$ in (5.2)), namely

$$H_\eta = \eta\sum_{i=1}^{N}(\sigma_i^+ + \sigma_i^-). \tag{5.18}$$

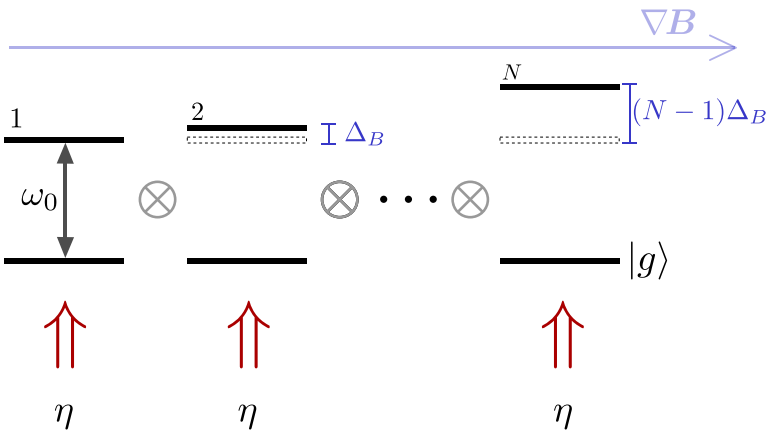

Figure 5.8: *Schematics illustrating driving with magnetic field gradient.* When driving with no phases, i.e. each atom with the same strength η, the excited state of the i-th atom is shifted by $\Delta_B(i-1)$ if a magnetic field gradient ∇B is present.

5.4.1 Two Atom Case

The complete Hamiltonian for two atoms when including the detuning due to the magnetic field gradient Δ_B, reads

$$H = \frac{\Delta}{2}(\sigma_z^{(1)} + \sigma_z^{(2)}) + \Delta_B(\sigma_2^+\sigma_2^-) + \eta(\sigma_1^+ + \sigma_2^+ + \sigma_1^- + \sigma_2^-) + \Omega(\sigma_1^+\sigma_2^- + \sigma_2^+\sigma_1^-). \tag{5.19}$$

It is still possible to compute the energy shifts that the states are subject to in this case. The respective shifts (without the dipole shifts included) are

$$\begin{aligned} &\langle G|\,\Delta_B\sigma_2^+\sigma_2^-\,|G\rangle = 0,\ \langle E|\,\Delta_B\sigma_2^+\sigma_2^-\,|E\rangle = \Delta_B, \\ &\langle A|\,\Delta_B\sigma_2^+\sigma_2^-\,|A\rangle = \langle S|\,\Delta_B\sigma_2^+\sigma_2^-\,|S\rangle = \frac{\Delta_B}{2}. \end{aligned} \tag{5.20}$$

These energetic shifts are schematically shown in Fig. 5.9. Note, that the levels $|S\rangle$, $|A\rangle$ and $|E\rangle$ get shifted to $|S'\rangle$, $|A'\rangle$ and $|E'\rangle$, respectively. However, one still aims to populate the state $|A\rangle$. From this brief calculation it is clear that the symmetric and asymmetric state get shifted in the same way due to the magnetic field gradient. Hence, the gradient does not further the energetic separation of these states. It does, however, introduce phases in the driving Hamiltonian. Since in the interaction picture the driving Hamiltonian H_η remains the same, this phase-imprinting is not obvious. Upon transforming the complete Hamiltonian into a partially time-dependent picture, though, time-dependent phases are introduced, yielding

$$H_\eta(t) = \eta(\sigma_1^+ + \sigma_2^+ e^{i\Delta_B\frac{t}{2}} + \sigma_1^- + \sigma_2^- e^{-i\Delta_B\frac{t}{2}}). \tag{5.21}$$

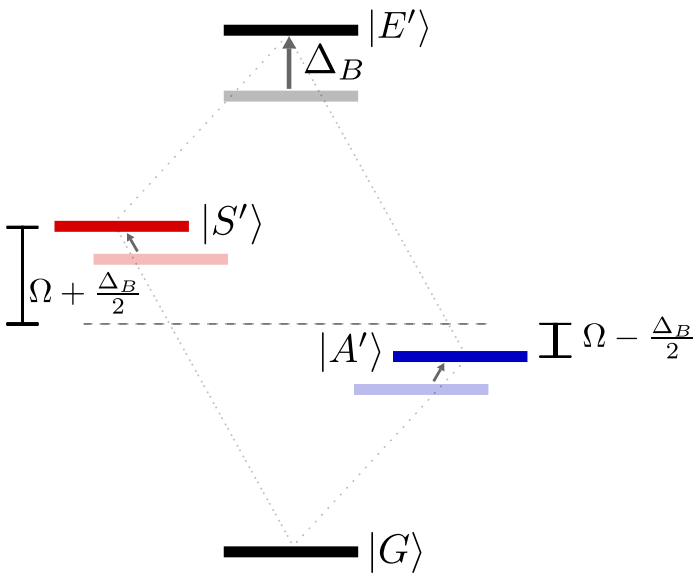

Figure 5.9: *Illustration of the energy shifts in the collective states of two atoms introduced by the magnetic field gradient and dipole-dipole interaction.*

This form of driving is not as effective as artificial phase-imprinting. At time $t = 0$, for example, the system will be driven in the symmetric instead of the asymmetric state since the phases vanish at that point. With a period that is dependent on the magnitude of Δ_B the Hamiltonian will transition from driving the symmetric state to driving the asymmetric state and back to driving the symmetric one. The idea now is that the period is fast enough such that the asymmetric state does not decay before being pumped again. Yet, the period has to be large enough for the state to actually accumulate population of significance during the time where the phases are close to matching the asymmetric state (namely $\Delta_B t/2 \approx \pi$). One therefore has to optimize the procedure with respect to Δ_B. Since this optimization requires computation of the full time evolution in dependence of Δ_B, it is best to perform it numerically.
Before moving on to numerical simulations, however, the idea of time-dependent phases will be extended to a larger chain of atoms.

5.4.2 Time-Dependent Phases

Combining the Hamiltonians from (5.17) and (5.18) yields a total Hamiltonian that is again time-independent, but can be transformed into a partially time-dependent picture, as it was done for the case of two atoms. This results in phases of the form used in (5.2), but time-dependent ones. Namely, the previously used phases become

$\phi_j = \phi_j(t) = -\Delta_B(j-1)t/2$ in the driving Hamiltonian that is then

$$H_\eta(t) = \sum_{j=1}^{N}(\sigma_j^+ e^{i\Delta_B(j-1)\frac{t}{2}} + \sigma_j^- e^{-i\Delta_B(j-1)\frac{t}{2}}). \tag{5.22}$$

Note, that this form of the driving Hamiltonian is of no further use but to illustrate the important point that the phases introduced by a magnetic field gradient are indeed time-dependent. Again, the phases vanish at certain (periodic) times which means that the Hamiltonian used to drive the system selects a symmetric (or close to symmetric) state rather than an asymmetric one. In order for such a symmetric state not to accumulate any population of relevance it is once more important to match the detuning of the Hamiltonian to the transition to the state of lowest decay rate according to the dipole shifts and the newly introduced shift by the magnetic field. Furthermore, the period of the phases has to be fast enough so that the population of the state with the lowest decay rate does not decay in the meantime, which does not pose much of a problem, though, since this state is indeed very long-lived.
The optimal detuning Δ in the Hamiltonian can be computed as in the case of artificial phases (5.15), however one has to include the shift introduced by the magnetic field, namely

$$\Delta = \langle\psi_{min}|\, \Delta_B \sum_j (j-1)\sigma_j^+\sigma_j^- + H_{dip}\, |\psi_{min}\rangle\,. \tag{5.23}$$

It shall be stated again at this point that the detuning introduced by the magnetic field is a parameter over which one has to optimize numerically since, unfortunately, there is no easy way to compute it analytically beforehand. This optimization will result in a detuning Δ_B that yields a slow enough period in the phases for the state with minimal decay rate to accumulate some population, yet fast enough that it does not decay when the phases do not match the symmetry. For larger numbers of atoms the optimal detuning Δ_B is smaller due to the scaling of the minimal decay rate with the atom number N (See Fig. 2.3), as it can also be seen in the following section.
Performing a scan over Δ_B, it is found that the population behaves symmetrically around zero as a function of the magnetic field detuning, as shown in Fig. 5.10(b). Furthermore, the efficiency of the procedure can be seen in Fig. 5.10(a).

5.4.3 Numerics

In order to show results even for larger chains of atoms one can again use the fact that the state of lowest decay rate only contains a single excitation. As can be seen in Fig. 5.11, though, larger numbers of atoms in principle yield the same results, but with even slower decay (saturation) due to the scaling of the minimal decay rate with the atom number. As the number of atoms grows, however, so does the overlap of the

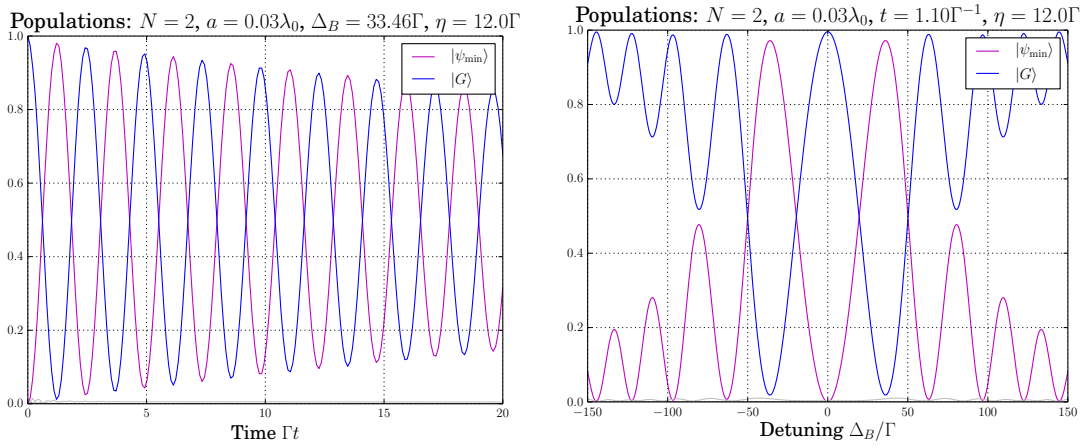

(a) (b)

Figure 5.10: *Driving the asymmetric state with a magnetic field gradient.* The graphs show the efficiency of the procedure when making use of the detuning introduced by the magnetic field for two atoms at a distance of $a = 0.03\lambda_0$. The pump has to be chosen quite strong ($\eta = 12\Gamma$), which does not pose a problem, however, since other transitions are so far off-resonant due to dipole shifts. (a) shows the time evolution when the detuning is optimized according to maximal population of the asymmetric state, i.e. the state of lowest decay rate. One can also see the beginning of the saturation due to decay, as it is expected. (b) presents the population of the asymmetric state as a function of the magnetic field detuning Δ_B. The time at which it has been plotted has been chosen optimal, i.e. the time of the first (largest) maximum of the population of the asymmetric state in (a).

energetic line shape functions of the states in the single-excitation manifold. It is hence important to decrease the distance in order to increase the separation of the lines due to the dipole shifts. Also note that it takes longer times for the state of minimal decay rate to accumulate population which, however, is no problem since this specific state grows more robust with the atom number, as it was just mentioned.
In conclusion, it can be stated that driving the state of the lowest decay rate is indeed possible, even without the physically not quite explicable artificial phases that have been used before by making use of a magnetic field gradient. Obviously, one can also use this scheme to perform a π-pulse similar to the way it has been done before (See Fig. 5.6).

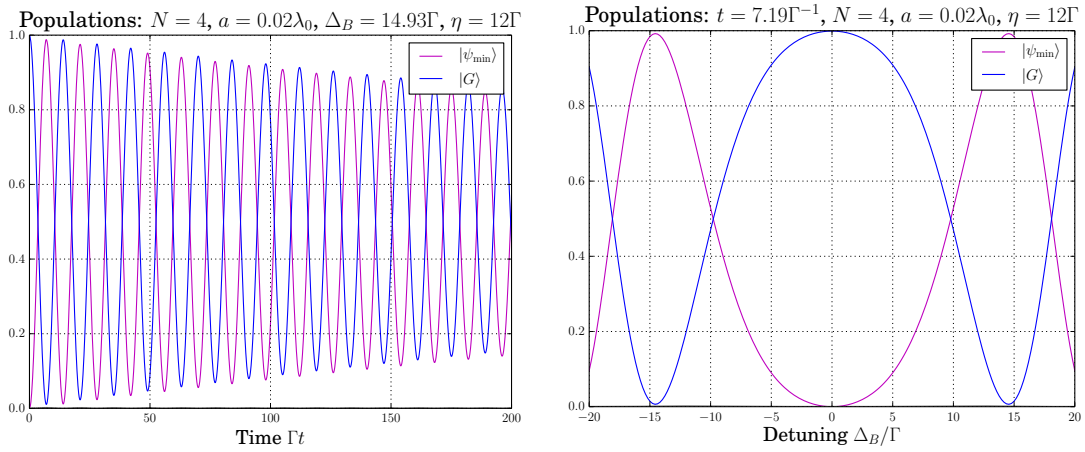

(a) (b)

Figure 5.11: *Driving the state of lowest decay rate in the single-excitation subspace.* Results for larger numbers of atoms, in this case $N = 4$ can be presented by reducing the entire Hilbert space to the single-excitation subspace. The distance has been reduced to $a = 0.02\lambda_0$ in order to enhance the dipole shifts. Once again, (a) shows the time evolution in the presence of driving, while (b) shows the population as a function of the detuning Δ_B.

Chapter 6

Conclusions and Outlook

Conclusions

A general discussion of the collective effects in an ensemble of quantum emitters has been provided and particularized to a chain of two-level atoms. Specifically, the collective decay of the system was considered. It was established that the theoretically minimal decay rate exhibits an exponential scaling with the number of atoms. This result was extended to realistic systems making use of numerical computations.
An enhanced method of Ramsey spectroscopy was discussed, yielding a better optimal sensitivity than in the standard quantum limit. This was done via state protection. Furthermore, the same mechanism of state protection was applied to spin-squeezed states, showing that it is possible to make spin squeezing more robust. Finally, a proposal that allows the direct preparation of a robust state, namely the eigenstate of the system with the longest lifetime was put forward. The efficiency of the proposed procedure was validated by numerical simulations and we further suggested to experimentally realize such a state preparation by employing a magnetic field gradient.

Future Investigations

Another common method in quantum metrology is the so-called Rabi spectroscopy [18]. Instead of two $\pi/2$-pulses with free time evolution in between (as in Ramsey spectroscopy), the Rabi method involves a single π-pulse that is applied over a certain time only. Also, instead of assuming the pulse to be instantaneous (rotation on the Bloch sphere), as it was done in this thesis, a continuous excitation can be considered. The idea is to formulate the phase-spread rotations in terms of a time-dependent excitation and use this in order to achieve a sensitivity better than what has been possible up to this point.
So far it has also not been considered that these methods of spectroscopy are actually subject to dephasing, be it laser-induced or caused by collisions of the atoms in the ensemble. As in the case of mutual decay, this dephasing can be described by a

Liouvillian operator. It is hence of interest, whether one could reduce this dephasing by symmetry manipulation of the states of the ensemble.
Furthermore, it has been shown that making use of quantum correlations, i.e. spin squeezing, in the Ramsey spectroscopy can lead to an enhancement of the sensitivity beyond the standard quantum limit [19–21]. It has been shown in this thesis, that state protection via the application of phase-spread rotations yields favourable results for both the Ramsey spectroscopy and the decay of a spin-squeezed state. This motivates the idea that including spin squeezing as well as state protection in the Ramsey procedure may very well lead to an even better sensitivity than when making use of only one of these enhancing effects.
In the matter of spin squeezing, it was also mentioned that there may be a more efficient method of protection for spin-squeezed states that have a Bloch vector far from aligned with the z-axis by using phase-spread rotations around the Bloch vector itself. It was explained, though, that this cannot be done via exact computation, but it might be possible to find an approximate form of the rotations.
One could also attempt a form of spectroscopy on the transition between the ground state of the system and the state of lowest decay rate in the single excitation manifold. This would possess the advantage of a vastly reduced decay rate, yet one would need to abandon all favourable scaling with the atom number, as the system is effectively reduced to one two-level transition.
It is also of uttermost interest to investigate the entanglement properties of the robust asymmetric state that is prepared via the procedure proposed in the last chapter. For the two atom case it has been shown that the state that is prepared is the asymmetric state, which is a Bell state (maximally entangled state). We will use tools like Quantum Fisher information or von Neumann entropy to analyze the entanglement properties of multipartite robust states [7]. If these investigations yield similar results for more atoms as those for only two, the robust state that is prepared would indeed be a robust highly (or even maximally) entangled state [22]. Since entanglement is a highly valuable resource in quantum information, the preparation of such a state would be applicable in a vast field of theoretical and experimental research.

Bibliography

[1] J. R. Johansson, P. D. Nation, and F. Nori. *Phys. Comm.*, 184:1234, 2013.

[2] R. Wynands and S. Weyers. Atomic fountain clocks. *Metrologia*, 42(3):S64, 2005.

[3] Z. Ficek and R. Tanaś. Entangled states and collective nonclassical effects in two-atom systems. *Physics Reports*, 372(5):369–443, 2002.

[4] L. Ostermann, H. Ritsch, and C. Genes. Protected state enhanced quantum metrology. *Phys. Rev. Lett.*, 111:123601, 2013.

[5] L. Ostermann, D. Plankensteiner, H. Ritsch, and C. Genes. Protected subspace ramsey spectroscopy. *Phys. Rev. A*, 90:053823, 2014.

[6] H. Zoubi and H. Ritsch. Optical properties of collective excitations for an atomic chain with vacancies. *The European Physical Journal D*, 66(11), 2012.

[7] D. Plankensteiner, L. Ostermann, H. Ritsch, and C. Genes. Preparation of robust multipartite entangled states. Work in progress, 2014.

[8] R. H. Dicke. Coherence in spontaneous radiation processes. *Physical Review*, 93(1):99, 1954.

[9] R. R. Puri. *Mathematical Methods of Quantum Optics*. Springer Berlin Heidelberg, 2001.

[10] T. Maier. Superradiant clock laser on an optical lattice. Master's thesis, Institut für Theoretische Physik, Universität Innsbruck, 2014.

[11] L. Ostermann, H. Zoubi, and H. Ritsch. Cascaded collective decay in regular arrays of cold trapped atoms. *Optics Express*, 20(28):29634–29645, 2012.

[12] H. Zoubi and H. Ritsch. Excitons and cavity polaritons for optical lattice ultracold atoms. *arXiv preprint arXiv:1301.6028*, 2013.

[13] H. Zoubi and H. Ritsch. Superradiant and dark exciton states in an optical lattice within a cavity. *Europhysics Letters*, 87(2), 2009.

[14] H. Zoubi and H. Ritsch. Lifetime and emission characteristics of collective electronic excitations in two-dimensional optical lattices. *Phys. Rev. A.*, 83(063831), 2011.

[15] H. Zoubi and H. Ritsch. Metastability and directional emission characteristics of excitons in 1d optical lattices. *EPL (Europhysics Letters)*, 90(2):23001, 2010.

[16] M. Kitagawa and M. Ueda. Squeezed spin states. *Phys. Rev. A.*, 47:5138, 1993.

[17] M. Orszag. *Quantum Optics*. Springer Berlin Heidelberg, 2008.

[18] I. I. Rabi. Space quantization in a gyrating magnetic field. *Physical Review*, 51:652–654, 1937.

[19] D. J. Wineland, J. J. Bollinger, W. M. Itano, F. L. Moore, and D. J. Heinzen. Spin squeezing and reduced quantum noise in spectroscopy. *Phys. Rev. A.*, 46(11):R6797–R6800, 1992.

[20] D. Oblak, P. G. Petrov, C. L. Alzar, et al. Quantum-noise-limited interferometric measurement of atomic noise: Towards spin squeezing on the cs clock transition. *Phys. Rev. A.*, 71(4):043807, 2005.

[21] D. Meiser, J. Ye, and M. J. Holland. Spin squeezing in optical lattice clocks via lattice-based QND measurements. *New Journal of Physics*, 10(7):073014, 2008.

[22] A. R. R. Carvalho, F. Mintert, and A. Buchleitner. Decoherence and multipartite entanglement. *Phys. Rev. Lett.*, 93(230501), 2004.